NATIONAL ADVISORY COMMITTEE FOR AERONAUTICS

TECHNICAL NOTE 1977

SUMMARY OF THE THEORETICAL LIFT, DAMPING-IN-ROLL, AND CENTER-OF-PRESSURE CHARACTERISTICS OF VARIOUS WING PLAN FORMS AT SUPERSONIC SPEEDS

By Robert O. Piland

Langley Aeronautical Laboratory
Langley Air Force Base, Va.

Washington
October 1949

NATIONAL ADVISORY COMMITTEE FOR AERONAUTICS

TECHNICAL NOTE 1977

SUMMARY OF THE THEORETICAL LIFT, DAMPING-IN-ROLL, AND CENTER-OF-PRESSURE CHARACTERISTICS OF VARIOUS WING PLAN FORMS AT SUPERSONIC SPEEDS

By Robert O. Piland

SUMMARY

The information for the determination of the theoretical lift, damping-in-roll, and center-of-pressure characteristics for a group of plan forms at supersonic speeds has been collected. This information is presented in three forms: first, equations; second, figures presenting generalized curves in which the quantities plotted are combinations of the geometric and aerodynamic parameters; and third, figures presenting curves for representative groups of specific configurations showing variation of the derivatives with Mach number. From this group several observations have been made as to the effect of taper ratio, angle of sweep, and aspect ratio on the values of the derivatives.

INTRODUCTION

The linearized theory for supersonic flow has been used by various investigators to develop expressions for the stability derivatives. The information is scattered, however, through a number of reports, not all of which use the same notation. A few of the more important derivatives are therefore collected herein for future comparison with experimental work and to aid designers by presenting the information in convenient form.

In order to make the paper more useful for purposes of comparison and design work, calculations were made for related groups of specific configurations. The results of these calculations are presented as plots of lift-curve slope, damping in roll, and center of pressure against Mach number. In addition, all available information is presented in the form of generalized figures in which the quantities plotted are combinations of the geometric and aerodynamic parameters.

SYMBOLS

x, y, z	rectangular coordinates (fig. 1)
p	angular velocity about x-axis (fig. 1)
V	flight speed
M	stream Mach number $\left(\frac{V}{\text{Speed of sound}}\right)$
μ	Mach angle
α	angle of attack (fig. 1)
$\beta = \sqrt{M^2 - 1}$	
ρ	density of air
b	span
c	local chord
c_r	root chord
c_t	tip chord
$\bar{c}$	mean aerodynamic chord $\left(\frac{2}{S}\int_0^{b/2} c^2 dy\right)$
λ	taper ratio (c_t/c_r)
S	wing area
A	aspect ratio (b^2/S)
Λ	angle of sweep of leading edge
Λ_t	angle of sweep of trailing edge
m	cotangent Λ
m_t	cotangent Λ_t
$N = 1 - \frac{4m}{A}$	
$\omega = \frac{4m}{A(1 + \lambda)}$	

$n = \frac{m}{m_t} = 1 - (1 - \lambda)\omega$

$k = \sqrt{1 - \beta^2 m^2}$

$E'(\beta m)$ complete elliptic integral of second kind with modulus k $\left(\int_0^{\pi/2} \sqrt{1 - k^2 \sin^2 z}\, dz\right)$

$F'(\beta m)$ complete elliptic integral of first kind with modulus k $\left(\int_0^{\pi/2} \frac{dz}{\sqrt{1 - k^2 \sin^2 z}}\right)$

$E''(\beta m) = \frac{1}{E'(\beta m)}$

$I(\beta m) = \frac{2(1 - \beta^2 m^2)}{(2 - \beta^2 m^2)E'(\beta m) - \beta^2 m^2 F'(\beta m)}$

L lift

l rolling moment

M' pitching moment about apex

C_L lift coefficient $\left(\frac{L}{\frac{1}{2}\rho V^2 S}\right)$

C_l rolling-moment coefficient $\left(\frac{l}{\frac{1}{2}\rho V^2 S b}\right)$

C_m pitching-moment coefficient $\left(\frac{M'}{\frac{1}{2}\rho V^2 S \bar{c}}\right)$

$C_{L_\alpha} = \left[\frac{\partial C_L}{\partial \alpha}\right]_{a \to 0}$

$C_{l_p} = \left[\frac{\partial C_l}{\partial \frac{pb}{2V}}\right]_{\frac{pb}{2V} \to 0}$

$C_{m_\alpha} = \left[\frac{\partial C_m}{\partial \alpha}\right]_{\alpha \to 0}$

$\frac{\bar{x}_{cp}}{\bar{c}}$ longitudinal distance between leading edge of mean aerodynamic chord and center of pressure due to lift, fraction of mean aerodynamic chord

$\frac{x_{cp}}{c_r}$ longitudinal distance between wing apex and center of pressure due to lift, fraction of root chord $\left(-\frac{C_{m_\alpha}}{C_{L_\alpha}}\frac{\bar{c}}{c_r}\right)$

Subscripts:

cp center of pressure

1,2 regions of wing panel in sketch in appendix

PRESENTATION OF RESULTS

Expressions for various stability derivatives have been obtained by several investigators (references 1 to 13) with the use of the linearized theory for supersonic flow. The equations for determining the theoretical lift, damping-in-roll, and center-of-pressure characteristics of various plan forms have been collected and are given in the appendix with a discussion of the range of applicability for each equation. All wings are considered to be of zero thickness and the equations are given with respect to axes having their origin at the leading edge with the x-axis coinciding with the root-chord line.

Table I lists the various specific wings considered according to their geometric characteristics. The equations and figure numbers given in the table serve as an index to the information presented in the paper. References from which the material was compiled are also listed in the table. The types of plan forms for which equations are given are shown in figure 2. Equations for a few plan forms not considered herein may be found in reference 13. Figures 3(a) to 3(f) illustrate the specific configurations considered. Figure 4 shows the variation of the elliptic-integral factors $E''(\beta m)$ and $I(\beta m)$ with βm and is to be used with the equations for the triangular, notched triangular, and swept tapered wings in the subsonic-leading-edge case ($\beta m < 1$).

Computational data obtained from the equations are presented in two forms. Generalized curves (figs. 5 to 10), in which the quantities plotted are combinations of the geometric and aerodynamic parameters, permit a rapid estimation of the value of a derivative for any specific wing whose general plan form is considered herein. Curves of the lift-curve slope, damping-in-roll, and center-of-pressure characteristics plotted against Mach number are presented in figures 11 to 16 for the specific configurations listed in table I.

DISCUSSION

From the variation of the derivatives (figs. 5 to 16) as predicted by linearized theory, several observations have been made as to the effect of sweep angle, taper ratio, and aspect ratio. The following effects were noted between Mach numbers of 1 and 2:

(1) For wings with subsonic leading edges, increase of sweep angle decreases the values of C_{L_α} and $-C_{l_p}$. At speeds at which the Mach line lies behind the leading edge, however, the lift-curve slope and the damping-in-roll values are greater with increased sweep. With increased angle of sweep, the center of pressure of a notched triangular wing moves rearward with respect to both the leading edge of the mean aerodynamic chord $\frac{\bar{x}_{cp}}{\bar{c}}$ and the apex of the wing $\frac{x_{cp}}{c_r}$.

(2) Because any change in taper ratio affects other wing parameters, the combined effects of taper ratio and sweep angle were noted with aspect ratio remaining constant. For a wing with a supersonic leading edge, an increase in taper ratio (ratio of tip chord to root chord) decreases the value of the lift-curve slope but increases the amount of damping in roll.

(3) Increase in aspect ratio increases values of the derivatives C_{L_α} and $-C_{l_p}$ and causes the center of pressure of the wing to move rearward. An exception is the triangular wing with a supersonic leading edge where the derivatives C_{L_α} and $-C_{l_p}$ are functions of Mach number alone and the center of pressure is constant at the two-thirds-chord point.

CONCLUDING REMARKS

A group of 52 specific wings representing various plan forms has been considered. The variations of the theoretical lift, damping-in-roll, and center-of-pressure characteristics of these wings with Mach number are presented. The equations from which these values were obtained are also presented.

From the figures presented, the effect of sweep, taper ratio, and aspect ratio may be noted. The lift-curve slope C_{L_α} decreased with increase in sweep angle when the leading edge was subsonic and increased when it was supersonic. Increased aspect ratio increased

the lift-curve slope. In the case of the triangular wing with a supersonic leading edge, however, C_{L_α} was independent of changes in sweep and aspect ratio.

The amount of damping in roll $-C_{l_p}$ was increased with increase of taper ratio, sweep angle, and aspect ratio except in the case of wings with subsonic leading edges in which an increase in sweep decreased the value of $-C_{l_p}$. Again an exception was noted in the case of the triangular wing with a supersonic leading edge for which $-C_{l_p}$ was not affected by changes in these parameters. The position of the center of pressure moved rearward with increase in sweep angle and aspect ratio, except in the case of the triangular wing in which it was constant at the two-thirds-chord point.

Langley Aeronautical Laboratory
National Advisory Committee for Aeronautics
Langley Air Force Base, Va., August 3, 1949

APPENDIX

EQUATIONS

Rectangular Wings

The equations for C_{L_α}, $\frac{x_{cp}}{c_r}$, and C_{l_p} for rectangular wings, which were obtained from references 1, 2, and 3, are as follows:

Limiting condition: $\frac{1}{2} \leqq \beta A \leqq 1$

$$\beta C_{L_\alpha} = \frac{4}{\pi \beta A}\left[(2\beta A - 1)\sin^{-1}\beta A + \beta A(\beta A - 2)\cosh^{-1}\frac{1}{\beta A} + (\beta A + 1)(1 - \beta^2 A^2)^{1/2}\right] \tag{1}$$

$$\frac{x_{cp}}{c_r} = \frac{1}{2}\left\{1 - 4\left[\frac{\sin^{-1}\beta A + \beta^2 A^2(3 - \beta A)\cosh^{-1}\frac{1}{\beta A} - (2\beta^2 A^2 - 2\beta A + 1)(1 - \beta^2 A^2)^{1/2}}{3\pi \beta A \beta C_{L_\alpha}}\right]\right\} \tag{2}$$

Limiting condition: $\beta A \geqq 1$

$$\beta C_{L_a} = 4 - \frac{2}{\beta A} \tag{3}$$

$$\frac{x_{cp}}{c_r} = \frac{3\beta A - 2}{6\beta A - 3} \tag{4}$$

$$\beta C_{l_p} = -\left(\frac{2}{3} - \frac{1}{\beta A} + \frac{1}{3\beta^2 A^2} + \frac{1}{12\beta^3 A^3}\right) \tag{5}$$

A group of rectangular wings, illustrated in figure 3(a), is considered. Variation of βC_{L_α}, $\frac{x_{cp}}{c_r}$, and $-\beta C_{l_p}$ with βA is shown in figure 5 and specific curves of C_{L_α}, $\frac{x_{cp}}{c_r}$, and $-C_{l_p}$ plotted against Mach number are shown in figure 11. Equations (3) to (5) are applicable for a range where the Mach line from a tip intersects the trailing edge ($\beta A > 1$). Equations (1) and (2) for C_{L_α} and $\frac{x_{cp}}{c_r}$ are applicable when a Mach line from the tip intersects the opposite edge between the midpoint of the side and the intersection of the side edge with the trailing edge $\left(1 > \beta A > \frac{1}{2}\right)$.

Unswept Tapered Wings

The equations for C_{L_α} and C_{l_p} for unswept tapered wings with supersonic leading edges which were obtained from reference 5 and an unpublished analysis at the Langley Laboratory are as follows:

Limiting condition: $\beta A \geq 2$

$$\beta C_{L_\alpha} = \frac{(2\beta m + \beta A)^2}{\pi \beta A(\beta^2 m^2 - 1)} - \frac{(2\beta m - \beta A)^2}{2\beta A(\beta m - 1)} + \frac{(2\beta m + \beta A)(\beta^2 m^2 - 2)\cos^{-1}\left(\frac{1}{\beta m}\right)}{\pi \beta A(\beta^2 m^2 - 1)^{3/2}} \tag{6}$$

$$\begin{aligned} \beta C_{l_p} = {} & \frac{-(2\beta m + \beta A)^4}{48\pi\beta^3 A^3(\beta^2 m^2 - 1)^3}\left[\frac{\beta^2 m^2(\beta^4 m^4 - 4\beta^2 m^2 + 8)\cos^{-1}\left(\frac{1}{\beta m}\right)}{(\beta^2 m^2 - 1)^{1/2}}\right. \\ & \left. + \frac{(3\beta^4 m^4 - 10\beta^2 m^2 - 8)}{3}\right] \\ & + \frac{(2\beta m - \beta A)^2}{4\beta A(\beta m - 1)}\left[\frac{(2\beta m - \beta A)^2(2\beta^2 m^2 - 6\beta m + 5)}{48\beta^2 A^2(\beta m - 1)^2}\right. \\ & \left. + \frac{(2\beta m - \beta A)(\beta m - 2)}{3\beta A(\beta m - 1)} + 1\right] \end{aligned} \tag{7}$$

The variation of βC_{L_α} and $-\beta C_{l_p}$ with βA for various taper ratios is shown in figure 6. The curves of C_{L_α} and $-C_{l_p}$, for a group of unswept tapered wings (fig. 3(b)), plotted against Mach number are shown in figures 12(a) to 12(d). Equations (6) and (7) are applicable when the Mach line from the apex intersects the trailing edge ($\beta A \geq 2$).

Triangular Wings

The equations for C_{L_α}, $\frac{x_{cp}}{c_r}$, and C_{l_p} for triangular wings with subsonic or supersonic leading edges which were obtained from references 6, 7, 8, and 9 are as follows:

(a) Subsonic leading edge

Limiting condition: $\beta A \leq 4$

$$\beta C_{L_\alpha} = \frac{\pi \beta A}{2} E''(\beta m) \tag{8}$$

$$\frac{x_{cp}}{c_r} = \frac{2}{3} \tag{9}$$

$$\beta C_{l_p} = -\frac{\pi \beta A}{32} I(\beta m) \tag{10}$$

(b) Supersonic leading edge

Limiting condition: $\beta A \geq 4$

$$\beta C_{L_\alpha} = 4 \tag{11}$$

$$\frac{x_{cp}}{c_r} = \frac{2}{3} \tag{12}$$

$$\beta C_{l_p} = -\frac{1}{3} \tag{13}$$

The variation of βC_{L_α}, $\frac{x_{cp}}{c_r}$, and $-\beta C_{l_p}$ with βA is shown in figure 7. The variation of C_{L_α}, $\frac{x_{cp}}{c_r}$, and $-C_{l_p}$ with Mach number is

shown in figure 13 for the configurations shown in figure 3(c). Equations (8) to (10) are applicable when the Mach line from the apex lies ahead of the leading edge ($\beta m < 1$). Equations (11) to (13) apply when the Mach lines from the apex lie behind the leading edge ($\beta m > 1$).

Notched Triangular Wings

The equations for C_{L_α}, $\frac{x_{cp}}{c_r}$, and C_{l_p} for notched triangular wings with subsonic or supersonic leading edges follow. They were obtained from references 10 and 11. No equation was given for C_{l_p} for wings with supersonic leading edges.

(a) Subsonic leading edge

Limiting conditions: $\beta m \leqq 1$

$\beta m \geqq |N|$

$$\beta C_{L_\alpha} = \beta A E''(\beta m)\frac{(1 - N)^{1/2}}{(1 + N)^{3/2}}\left[\cos^{-1}(-N) + N(1 - N^2)^{1/2}\right] \tag{14}$$

$$\frac{x_{cp}}{c_r} = \frac{N(4 - N^2) + (2 + N^2)(1 - N^2)^{-1/2}\cos^{-1}(-N)}{3(1 - N^2)\left[N + (1 - N^2)^{-1/2}\cos^{-1}(-N)\right]} \tag{15}$$

$$\beta C_{l_p} = \frac{-\beta A I(\beta m)}{48}\frac{(1 - N)^{1/2}}{(1 + N)^{7/2}}\left[3(4N^2 + 1)\cos^{-1}(-N) + N(2N^2 + 13)(1 - N^2)^{1/2}\right] \tag{16}$$

(b) Supersonic leading edge

Limiting conditions: $\beta m \geqq 1$

$1 \geqq N \geqq -1$

$$\beta C_{L_\alpha} = \frac{8\beta m}{\pi(N + 1)}\left[\frac{\cos^{-1}\left(\frac{-N}{\beta m}\right)}{(\beta^2 m^2 - N^2)^{1/2}} + \frac{N\cos^{-1}\left(\frac{1}{\beta m}\right)}{(\beta^2 m^2 - 1)^{1/2}}\right] \tag{17}$$

$$\frac{x_{cp}}{c_r} = \frac{\dfrac{(2\beta^2m^2 - N^2 - N^4)\cos^{-1}\left(\frac{-N}{\beta m}\right)}{(1 - N^2)(\beta^2m^2 - N^2)^{3/2}} + \dfrac{N(3 - N^2)\cos^{-1}\frac{1}{\beta m}}{(1 - N^2)(\beta^2m^2 - 1)^{1/2}} + \dfrac{N}{(\beta^2m^2 - N^2)}}{3\left[\dfrac{-\cos^{-1}\left(\frac{-N}{\beta m}\right)}{(\beta^2m^2 - N^2)^{1/2}} + \dfrac{N\cos^{-1}\frac{1}{\beta m}}{(\beta^2m^2 - 1)^{1/2}}\right]} \qquad (18)$$

The variation of βC_{L_α}, $\frac{x_{cp}}{c_r}$, $\frac{\bar{x}_{cp}}{\bar{c}}$, and $-\beta C_{l_p}$ with βm for various values of βA is given in figure 8. The parameters C_{L_α}, $\frac{x_{cp}}{c_r}$, $\frac{\bar{x}_{cp}}{\bar{c}}$, and $-C_{l_p}$ for the group of wings illustrated in figure 3(d), plotted against Mach number, are shown in figures 14(a), 14(b), and 14(c). Equations (14) to (16) are applicable for a range of Mach numbers for which the Mach line from the apex lies ahead of the leading edge ($\beta m < 1$) and the Mach line from the trailing edge of the root chord lies behind the trailing edge ($\beta m \geq N$). When this latter condition is violated a value of the derivative is obtained which has the significance of an upper limit (reference 10). This region ($\beta m < N$) is indicated by a dashed curve. Equations (17) and (18) for C_{L_α} and $\frac{x_{cp}}{c_r}$, respectively, are applicable when the Mach line from the apex intersects the trailing edge of the wing. The relation between $\frac{x_{cp}}{c_r}$ and $\frac{\bar{x}_{cp}}{\bar{c}}$ is given by the expression

$$\frac{\bar{x}_{cp}}{\bar{c}} = \frac{3}{2}\left(\frac{x_{cp}}{c_r} - \frac{A}{12m}\right)$$

Swept Untapered Wings

The equations for C_{L_α} and C_{l_p} for the case in which the Mach line from the apex lies on the leading edge ($\beta m = 1$) were obtained by modifying equations in reference 12 in the following manner:

For the lift case,

$$C_{L_\alpha} = \frac{\partial}{\partial \alpha}\left(C_{L_1} + C_{L_2}\right) \qquad (a)$$

where subscripts 1 and 2 refer to the regions of the wing panel shown in the following sketch:

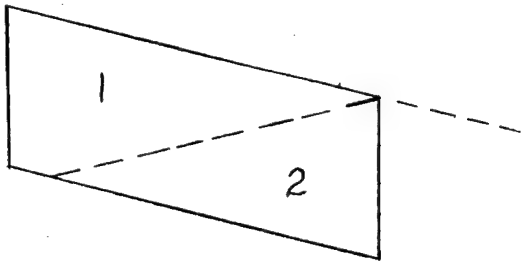

If the taper ratio is 1 and the Mach line coincides with the leading edge ($\beta m = 1$), equation (9) of reference 12 becomes

$$C_{L_1} = \frac{8m^2 c_r{}^2 \alpha}{\pi S}\int_0^{\frac{b-mc}{b+mc}} \frac{d\nu}{(1-\nu)^2\sqrt{1-\nu^2}} + \frac{8b^2\alpha}{\pi S}\int_{\frac{b-mc}{b+mc}}^{1} \frac{d\nu}{(1+\nu)^2\sqrt{1-\nu^2}} \qquad (b)$$

and equation (12) of reference 12 becomes

$$C_{L_2} = \frac{8m\alpha}{\pi S}\int_{\frac{b}{2}-\frac{mc}{2}}^{\frac{b}{2}} \int \sqrt{\frac{b-2y}{mx+y}}\, dx\, dy \qquad (c)$$

Performing the operations indicated in equations (a), (b), and (c) yields an expression for C_{L_α} in terms of β and A. Similarly, modifying equation (19) of reference 12 in the preceding manner gives

$$C_{l_1} = \frac{-8m^4 c_r{}^4 p}{3SbV}\int_0^{\frac{b-mc}{b+mc}} \frac{\nu^2 d\nu}{(1-\nu)^4\sqrt{1-\nu^2}} - \frac{8b^3 p}{3VS}\int \frac{\nu^2 d\nu}{(1+\nu)^4\sqrt{1-\nu^2}} \qquad (d)$$

and equation (23) of reference 12 becomes

$$C_{l_2} = \frac{8mp}{3\pi VSb} \int_{\frac{b}{2}-\frac{mc}{2}}^{b/2} \int_{\beta\left(\frac{b}{2}-y\right)+\frac{b}{2m}}^{\frac{y}{m+c}} \frac{y\left(3mx - y - b\right)\sqrt{\frac{b}{2} - y}}{\sqrt{2(mx + y)}} \, dx \, dy \qquad (e)$$

The amount of damping contributed by the tip section, however, is seen to be negligible and consequently the expression derived for this region has been omitted from the expression for C_{l_p}. Performing the operations indicated in equation (d) and taking the derivative of C_l with respect to $\frac{pb}{2V}$ give the equation for C_{l_p}.

The equations for C_{L_α} and C_{l_p} derived are as follows:

Condition of applicability: $\beta m = 1$

$$\beta C_{L_\alpha} = \frac{1}{\pi}\left[\frac{1}{\sqrt{\beta A}}\left(\frac{10\beta A}{3} + 2\right) - \frac{16}{3\beta A} + \beta A\left(1 + \frac{1}{\beta A}\right)^2 \cos^{-1}\frac{\beta A - 1}{\beta A + 1}\right] \qquad (19)$$

$$\beta C_{l_p} = -\frac{16}{3\pi}\left[\sqrt{\beta A}\left(\frac{1}{7} - \frac{1}{15\beta A} - \frac{1}{15\beta^2 A^2} + \frac{1}{7\beta^3 A^3}\right) - \frac{8}{105\beta^3 A^3}\right] \qquad (20)$$

The equations for C_{L_α} and C_{l_p} for a swept untapered wing for the case in which the Mach line from the apex crosses the trailing edge $\left(\beta > \frac{2}{A} + \frac{1}{m}\right)$ were obtained from an unpublished analysis by Mr. Sidney M. Harmon of the Langley Stability Research Division and are as follows:

Limiting condition: $\beta > \frac{2}{A} + \frac{1}{m}$

$$\beta C_{L_\alpha} = \frac{4}{\beta A\sqrt{\beta^2 m^2 - 1}}\left[\frac{\beta^2 m^2(\beta^2 m^2 - 2)\sin^{-1}\frac{1}{\beta m}}{\pi(\beta^2 m^2 - 1)} - \frac{\beta^2 m^2}{\pi\sqrt{\beta^2 m^2 - 1}} - \frac{\beta^3 m^3}{2(\beta^2 m^2 - 1)} + \beta A \beta m\right] \qquad (21)$$

$$\beta C_{l_p} = \frac{\beta^5 m^5(-2\beta^3 m^3 + 4\beta^2 m^2 + 2\beta m - 9)}{12\beta^3 A^3(\beta m - 1)^2(\beta^2 m^2 - 1)^{3/2}} - \frac{\beta^3 m^3}{3\beta^2 A^2(\beta^2 m^2 - 1)^{3/2}}$$

$$+ \frac{\beta^3 m^3}{\beta A(\beta^2 m^2 - 1)^{3/2}} \frac{-2\beta m}{3\sqrt{\beta^2 m^2 - 1}} + \frac{\beta^4 m^4(3\beta^4 m^4 - 10\beta^2 m^2 - 8)}{9\pi\beta^3 A^3(\beta^2 m^2 - 1)^3}$$

$$+ \frac{\beta^4 m^4(\beta^6 m^6 - 4\beta^4 m^4 + 8\beta^2 m^2)\cos^{-1}\frac{1}{\beta m}}{3\pi\beta^3 A^3(\beta^2 m^2 - 1)^{7/2}} \qquad (22)$$

The variation of βC_{L_α} and $-\beta C_{l_p}$ with βm for various values of βA is shown in figure 9. No equation is available for the case in which the Mach line from the apex cuts the side edge of the wing; consequently the points obtained from equations (19) and (20) have been faired to the curves obtained from equations (21) and (22). These regions are indicated by dashed lines. No equations were available for $\frac{x_{cp}}{c_r}$ for swept untapered wings. Curves of C_{L_α} and $-C_{l_p}$, varying with Mach number, for the swept untapered wings shown in figure 3(e) are presented in figures 15(a), 15(b), and 15(c).

Swept Tapered Wings

Equations for C_{L_α} and C_{l_p} for swept tapered wings obtained from reference 12 and from the previously mentioned unpublished analysis follow (no equation is given for C_{l_p} for the case of a wing with a supersonic leading edge):

(a) Subsonic leading edge

Limiting condition: For $\beta A(1 + \lambda) \geq 2$, $\frac{\beta A(1 + \lambda)}{\beta A(1 + \lambda) + 4(1 - \lambda)} \leq \beta m \leq 1$

For $\beta A(1 + \lambda) < 2$, $\frac{\beta A(1 + \lambda)}{\beta A(1 + \lambda) + 4(1 - \lambda)} \leq \beta m \leq \frac{\beta A(1 + \lambda)}{4 - \beta A(1 + \lambda)}$

$$n = \frac{A(1 + \lambda) + 4m(\lambda - 1)}{A(1 + \lambda)} \qquad \omega = \frac{4m}{A(1 + \lambda)}$$

$$\beta C_{L_\alpha} = \frac{\beta A}{E'(\beta m)} \left(\frac{\omega^2}{(1 - n^2)^{3/12}} \left[\sin^{-1} n - \sin^{-1} \frac{(\beta m + 1)(n^2 - 1) + \omega(\beta m n + 1)}{\omega(\beta m + n)} \right] \right.$$

$$+ \frac{(1 + \beta m)^{1/2}}{(1 - \beta m)^{3/2}} \cos^{-1} \frac{1 + \beta m n + \omega(\beta m - 1)}{\beta m + n} + \frac{n\omega^2}{1 - n^2}$$

$$\left. + \frac{[\omega n(\beta m - 1) + \beta m(n^2 - 1)](1 + \beta m)^{1/2}}{(\beta m + n)(n^2 - 1)(\beta m - 1)} \left\{ (\omega + n - 1)\left[(\beta m + 1)(n + 1) + \omega(\beta m - 1) \right] \right\}^{1/2} \right)$$

$$+ \frac{4\beta A}{\pi(1 + \beta m)^{1/2}} \left(\frac{(1 + n + \omega)^2}{4(1 + n)^{3/2}} \cos^{-1} \frac{(n + \omega)(\beta m - n) + 2(1 - \omega) + \beta m + n}{(1 + n + \omega)(\beta m + n)} \right.$$

$$- \frac{1}{(1 - \beta m)^{3/2}} \cos^{-1} \frac{1 + \beta m n + \omega(\beta m - 1)}{\beta m + n}$$

$$\left. + \frac{(1 + \beta m)(1 + n) - \omega(1 - \beta m)}{2(\beta m + n)(1 - \beta m)(1 + n)} \left\{ (\omega - n + 1)\left[(\beta m + 1)(n + 1) + \omega(\beta m - 1) \right] \right\}^{1/2} \right) \qquad (23)$$

$$\beta C_{l_p} = \frac{I(\beta m)\beta A}{8}\left(\frac{\omega^4 n(2n^2+13)}{6(n^2-1)^3} + \frac{\omega^4(4n^2+1)}{2(1-n^2)^{7/2}}\left[\sin^{-1}\frac{(\beta m+1)(n^2-1)+\omega(\beta mn+1)}{\omega(\beta m+n)} - \sin^{-1}n\right] - \frac{(4\beta^2m^2+1)(\beta m+1)^{1/2}}{2(1-\beta m)^{7/2}}\cos^{-1}\frac{\omega(\beta m-1)+\beta mn+1}{\beta m+n}\right.$$

$$- \omega(\beta m+1)^{1/2}\left\{\frac{(1-\omega+\beta m)\left[n(1+\beta m-\omega)(6n^4+10n^2-1)+3(1-9n^2-2n^4)(n+\beta mn+\beta m\omega)\right]+n(2n^2+13)(n+\beta mn+\beta m\omega)^2}{6(n^2-1)^3(\beta m+n)^3}\right\}\left\{(\omega+n-1)\left[(\beta m+1)(n+1)+\omega(\beta m-1)\right]\right\}^{1/2}$$

$$\left. + \left\{\frac{(1-\omega+\beta m)\left[m\beta(1-\omega+\beta m)(1-10\beta^2m^2-6\beta^4m^4)+3(1-9\beta^2m^2-2\beta^4m^4)(n+\beta mn+\beta m\omega)\right]-\beta m(2\beta^2m^2+13)(n+\beta mn+\beta m\omega)^2}{6(\beta m-1)^3(\beta m+1)^{3/2}(\beta m+n)^3}\right\}\left\{(\omega+n-1)\left[(\beta m+1)(n+1)+\omega(\beta m-1)\right]\right\}^{1/2}\right)$$

$$- \frac{\beta A}{6\pi(\beta m+1)^{3/2}}\left(\left\{\frac{-4(n+1)(1+\beta m-\omega)(1-\beta m)(1+5\beta m)+5\left[(1-n+2\beta m)(n+1-\omega)(1-\beta m)^2+2\beta m(n+1)^2(1+3\beta m)\right]}{3(1+n)^2(1-\beta m)^2(\beta m+n)^3}\right\}\left[\beta m(n+\omega)^2-(\omega-1)^2+(n^2-\beta m)\right]^{3/2}\right.$$

$$+ \left\{\frac{5(1+n-\omega)^2(1-n+2\beta m)+4(1+n)\left[(2-3\omega+2\beta m)(1+n)+2\omega^2\right]}{8(1+n)^3}\right\}\left\{\frac{n(n-\beta m)-(2+n)(1-\omega)-\beta m(1-\omega)}{(\beta m+n)^2}\left\{(\omega+n-1)\left[(\beta m+1)(n+1)+\omega(\beta m-1)\right]\right\}^{1/2}\right.$$

$$\left. + \frac{(n+1+\omega)^2}{2(n+1)^{1/2}}\cos^{-1}\frac{\beta m(1+\omega)+(2+n)(1-\omega)-n(n-\beta m)}{(n+1+\omega)(\beta m+n)}\right\} + \frac{(1+3\beta m)(4\beta^2m^2+1)}{(1-\beta m)^3}\left\{\frac{1+\beta mn-\omega(1-\beta m)}{(\beta m+n)^2}\left\{(\omega+n-1)\left[(\beta m+1)(n+1)+\omega(\beta m-1)\right]\right\}^{1/2}\right.$$

$$\left.\left. - \frac{1}{(1-\beta m)^{1/2}}\cos^{-1}\frac{\omega(\beta m-1)+\beta mn+1}{\beta m+n}\right\}\right) \qquad (24)$$

(b) Supersonic leading edge

Limiting condition: $\beta > \frac{2}{A} + \frac{1+n}{2m}$

$$\beta C_{L_\alpha} = \frac{1}{(\beta^2m^2-1)^{1/2}}\left\{\frac{(4\beta m-\beta An+\beta A)^2}{2\pi\beta A(1-n^2)}\left[n\cos^{-1}\frac{1}{\beta m} + \frac{(\beta^2m^2-1)^{1/2}\cos^{-1}\frac{-n}{\beta m}}{(\beta^2m^2-n^2)}\right] - \frac{(4\beta m+\beta An-\beta A)^2(\beta m+1)^{1/2}}{4\beta A(1-n)(\beta m+n)^{1/2}}\right\} \qquad (25)$$

The variation of βC_{L_α} and $-\beta C_{l_p}$ with βm for various values of βA for swept tapered wings of taper ratio 0.5 is shown in figure 10. Curves of C_{L_α} and $-C_{l_p}$ plotted against Mach number are shown in figure 16 for the configurations of figure 3(f). Equations (23) (for C_{L_α}) and (24) (for $-C_{l_p}$) are applicable for the case in which the Mach line from the apex lies ahead of the leading edge and the Mach line from the trailing edge of the root chord lies behind the trailing edge. Violation of the latter condition will give values of the derivative which have the significance of an upper limit (reference 12). These regions are indicated by the dashed parts of the curves. Equation (25) (for C_{L_α}) is applicable when the Mach line from the apex intersects the trailing edge $\left(\beta > \frac{2}{A} + \frac{1 + n}{m}\right)$. The two parts of the curves obtained from the equations for C_{L_α} have been faired together over the region where the Mach line from the tip crosses the side edge of the wing.

REFERENCES

1. Lagerstrom, P. A., and Graham, Martha E.: Low Aspect Ratio Rectangular Wings in Supersonic Flow. Rep. No. SM-13110, Douglas Aircraft Co., Inc., Dec. 1947.

2. Bonney, E. Arthur: Aerodynamic Characteristics of Rectangular Wings at Supersonic Speeds. Jour. Aero. Sci., vol. 14, no. 2, Feb. 1947, pp. 110-116.

3. Lagerstrom, P. A., and Graham, Martha E.: Some Aerodynamic Formulas in Linearized Supersonic Theory for Damping in Roll and Effect of Twist for Trapezoidal Wings. Rep. No. SM-13200, Douglas Aircraft Co., Inc., March 12, 1948.

4. Harmon, Sidney M.: Stability Derivatives of Thin Rectangular Wings at Supersonic Speeds. Wing Diagonals ahead of Tip Mach Lines. NACA TN 1706, 1948.

5. Tucker, Warren A., and Nelson, Robert L.: The Effect of Torsional Flexibility on the Rolling Characteristics at Supersonic Speeds of Tapered Unswept Wings. NACA TN 1890, 1949.

6. Brown, Clinton E.: Theoretical Lift and Drag of Thin Triangular Wings at Supersonic Speeds. NACA Rep. 839, 1946.

7. Ribner, Herbert S., and Malvestuto, Frank S., Jr.: Stability Derivatives of Triangular Wings at Supersonic Speeds. NACA TN 1572, 1948.

8. Puckett, Allen E.: Supersonic Wave Drag of Thin Airfoils. Jour. Aero. Sci., vol. 13, no. 9, Sept. 1946, pp. 475-484.

9. Brown, Clinton E., and Adams, Mac C.: Damping in Pitch and Roll of Triangular Wings at Supersonic Speeds. NACA Rep. 892, 1948.

10. Malvestuto, Frank S., Jr., and Margolis, Kenneth: Theoretical Stability Derivatives of Thin Sweptback Wings Tapered to a Point with Sweptback or Sweptforward Trailing Edges for a Limited Range of Supersonic Speeds. NACA TN 1761, 1949.

11. Puckett, A. E., and Stewart, H. J.: Aerodynamic Performance of Delta Wings at Supersonic Speeds. Jour. Aero. Sci., vol. 14, no. 10, Oct. 1947, pp. 567-578.

12. Malvestuto, Frank S., Jr., Margolis, Kenneth, and Ribner, Herbert S.: Theoretical Lift and Damping in Roll of Thin Sweptback Wings of Arbitrary Taper and Sweep at Supersonic Speeds. Subsonic Leading Edges and Supersonic Trailing Edges. NACA TN 1860, 1949.

13. Jones, Arthur L., and Alksne, Alberta: The Damping Due to Roll of Triangular, Trapezoidal, and Related Plan Forms in Supersonic Flow. NACA TN 1548, 1948.

TABLE I.- CONFIGURATIONS AND INDEX TO INFORMATION

Plan form	Reference	Wing	Angle of sweep		Aspect ratio	Taper ratio	Equation			Figure		
			L.E. (Λ) (deg)	T.E. (Λ_t) (deg)			C_{L_α}	$\frac{x_{cp}}{c_r}$	C_{l_p}	Configuration	Generalized curves	Data
Rectangular	1, 2, 3, 4	1	0	0	2	1	(1), (3)	(2), (4)	(5)	3(a)	5	11(a), 11(b)
		2	0	0	3	1						
		3	0	0	4	1						
		4	0	0	6	1						
		5	0	0	8	1						
Unswept tapered	5 and an unpublished analysis	6	35	-35	2	.2	(6)		(7)	3(b)	6	12(d)
		7	24.5	-24.5	2	.4						12(c)
		8	18.7	-18.7	2	.6						12(b)
		9	12.5	-12.5	2	.8						12(a)
		10	23	-23	3	.2						12(d)
		11	16	-16	3	.4						12(c)
		12	11.9	-11.9	3	.6						12(b)
		13	8.2	-8.2	3	.8						12(a)
		14	14.5	-14.5	4	.2						12(d)
		15	10	-10	4	.4						12(c)
		16	7.5	-7.5	4	.6						12(b)
		17	5	-5	4	.8						12(a)
		18	6.3	-6.3	6	.2						12(d)
		19	4.5	-4.5	6	.4						12(c)
		20	3	-3	6	.6						12(b)
		21	2.1	-2.1	6	.8						12(a)
Triangular	6, 7, 8, 9	22	75.9	0	1	0	(8), (11)	(9), (12)	(10), (13)	3(c)	7	13
		23	63.4	0	2	0						
		24	60	0	2.308	0						
		25	53.1	0	3	0						
		26	45	0	4	0						
Notched triangular	10, 11	27	45	26.5	8	0	(14), (17)	(15), (18)	(16)	3(d)	8	14(a)
		28	53.1	34.5	6	0						14(a)
		29	63.4	44.5	4	0						14(a)
		30	69.4	53.5	3	0						14(b)
		31	45	18	6	0						14(b)
		32	60	22.4	3	0						14(c)
		33	60	36.5	4	0						14(c)
		34	60	46.8	6	0						14(c)
Swept untapered	12 and an unpublished analysis	35	30	30	2	1	(19), (21)		(20), (22)	3(e)	9	15(a)
		36	30	30	4	1						15(a)
		37	30	30	6	1						15(a)
		38	45	45	2	1						15(b)
		39	45	45	4	1						15(b)
		40	45	45	6	1						15(b)
		41	60	60	2	1						15(c)
		42	60	60	3	1						15(c)
		43	60	60	4	1						15(c)
Swept tapered	12 and an unpublished analysis	44	30	-5	2	.5	(23), (25)		(24)	3(f)	10	16(a)
		45	30	14	4	.5						16(a)
		46	30	19	6	.5						16(a)
		47	45	18.5	2	.5						16(b)
		48	45	34.4	4	.5						16(b)
		49	45	38.8	6	.5						16(b)
		50	60	48	2	.5						16(c)
		51	60	52.5	3	.5						16(c)
		52	60	54.5	4	.5						16(c)

NACA

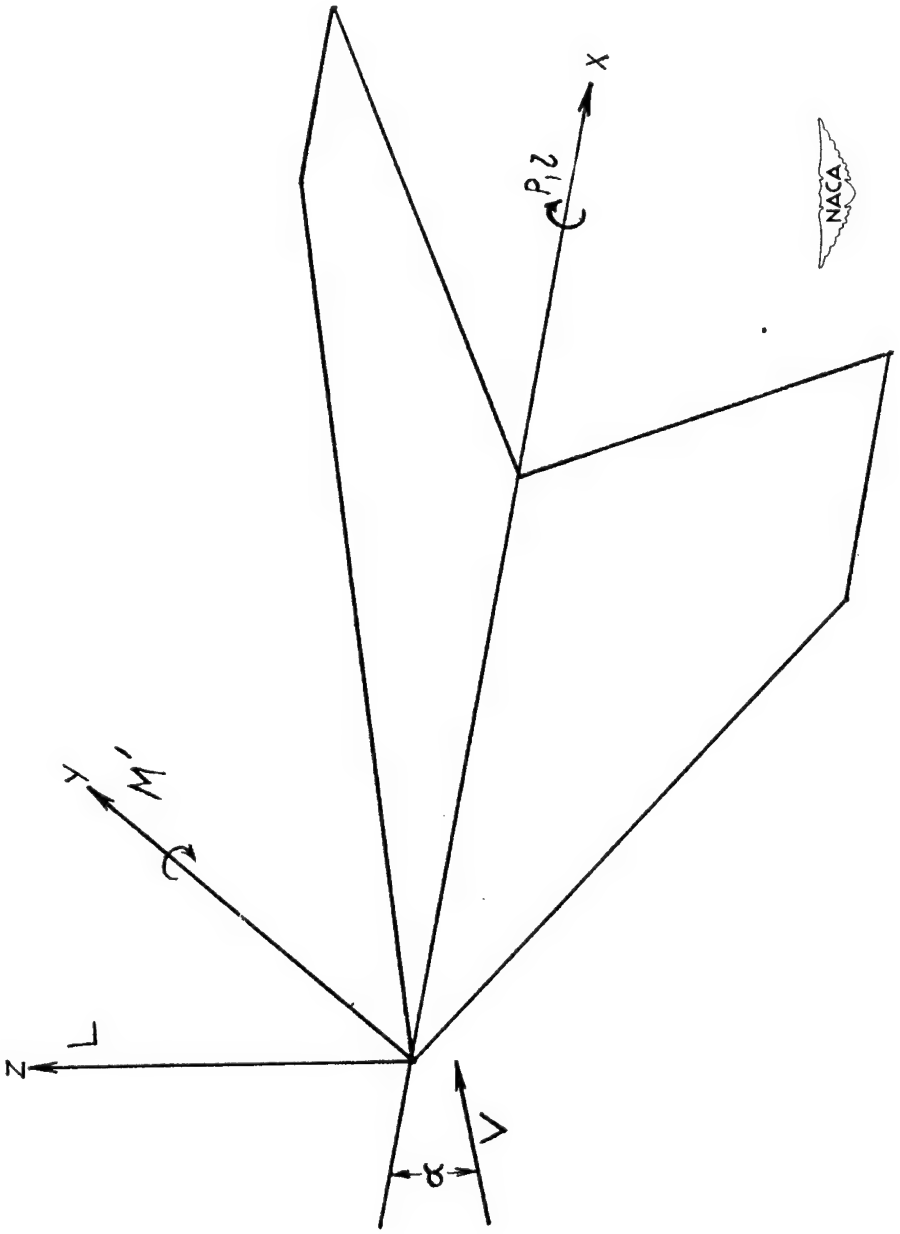

Figure 1.- Axes and notations used in equations.

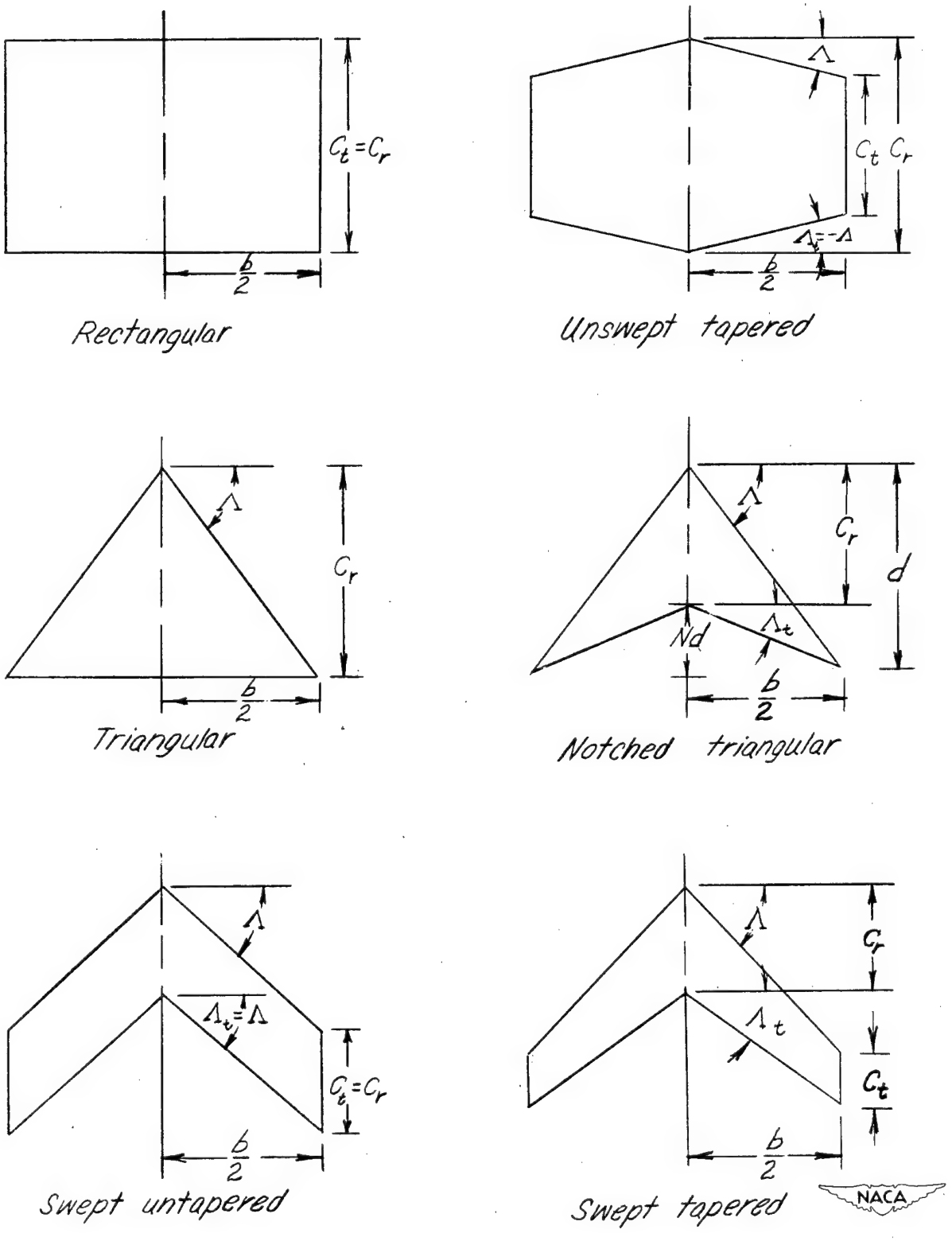

Figure 2.– Various types of plan form for which equations are given.

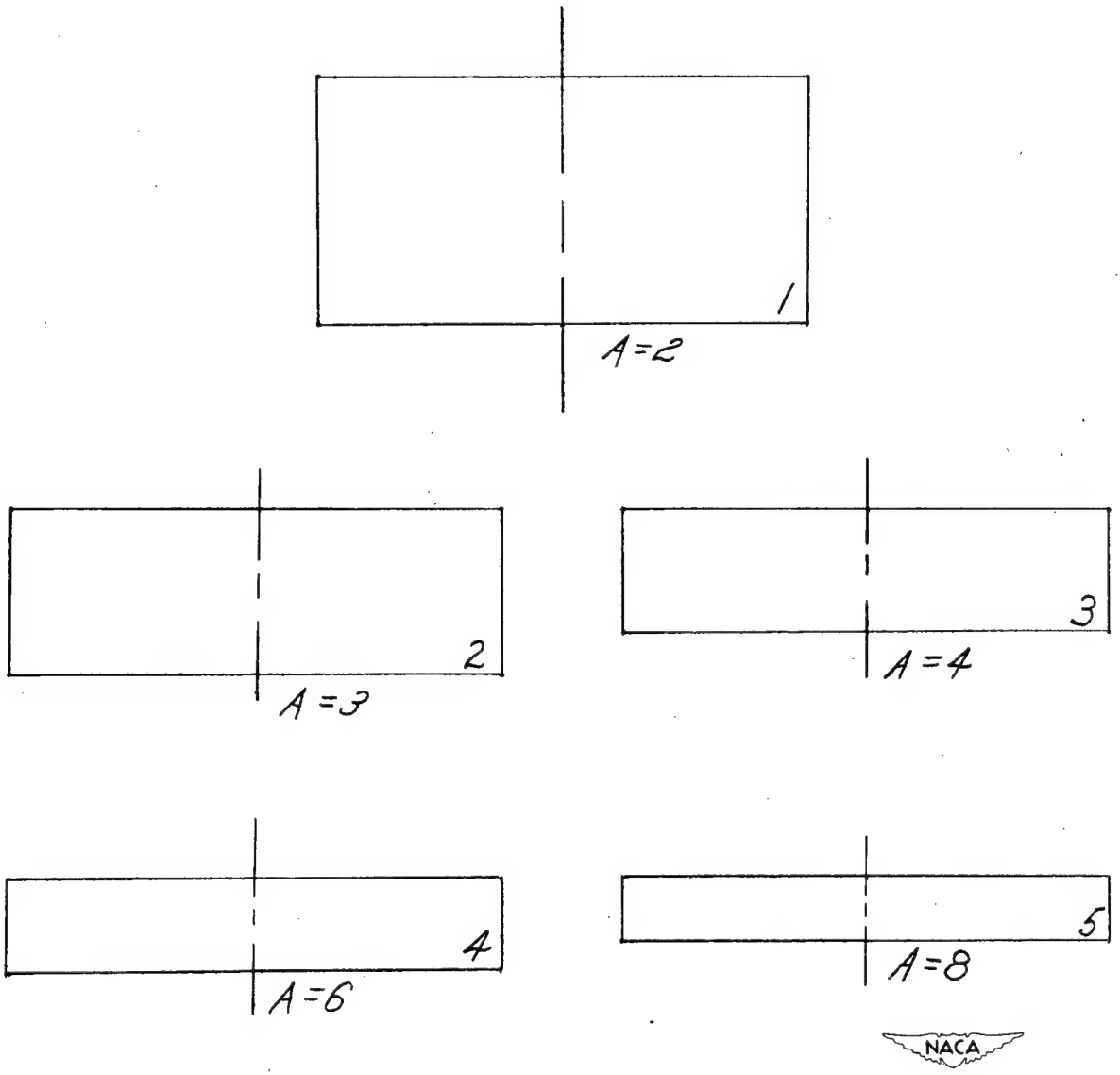

(a) Rectangular wings.

Figure 3.– Specific configurations for which curves are presented. Numbers within plan forms correspond to wing numbers in table I.

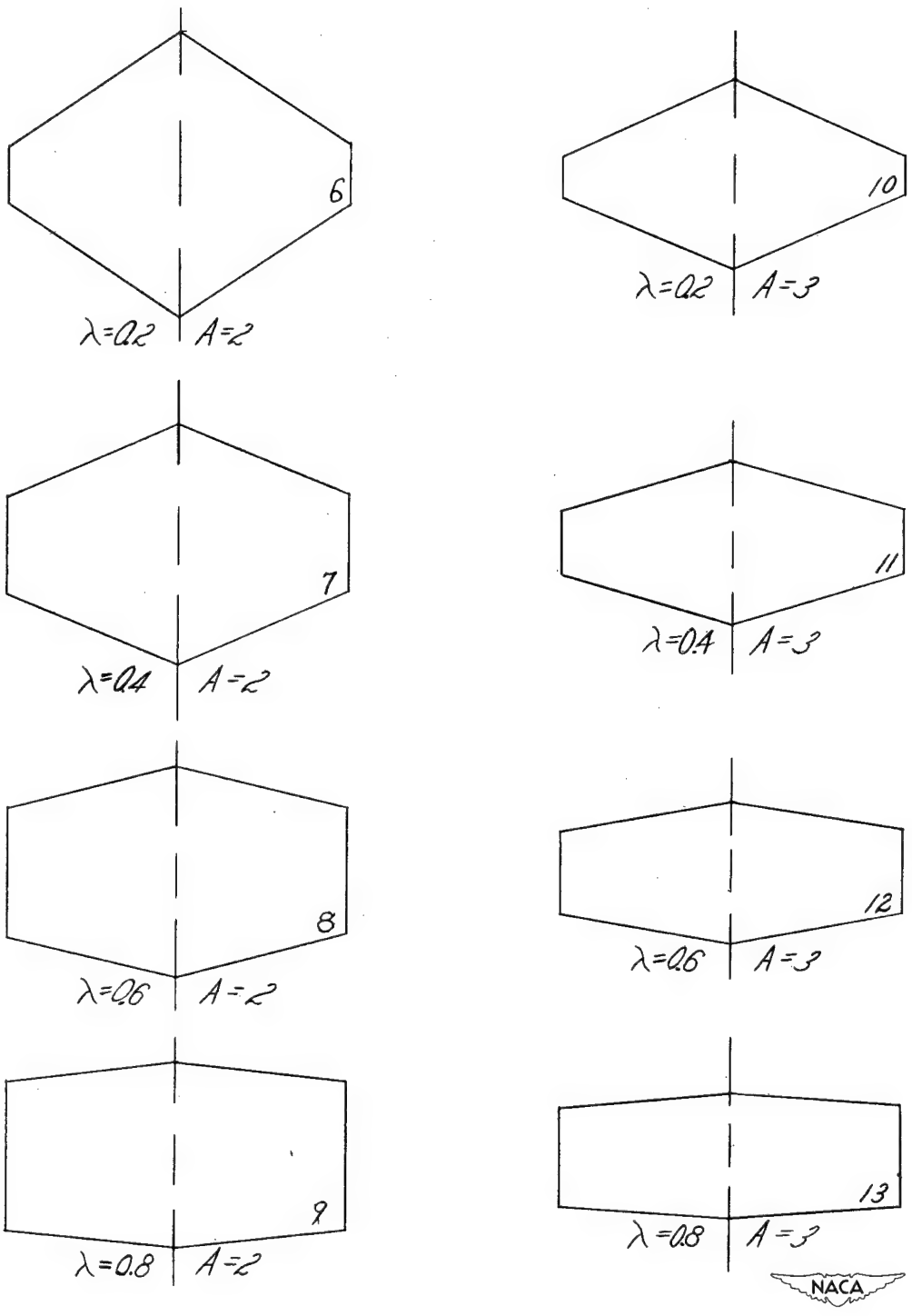

(b) Unswept tapered wings.

Figure 3.– Continued.

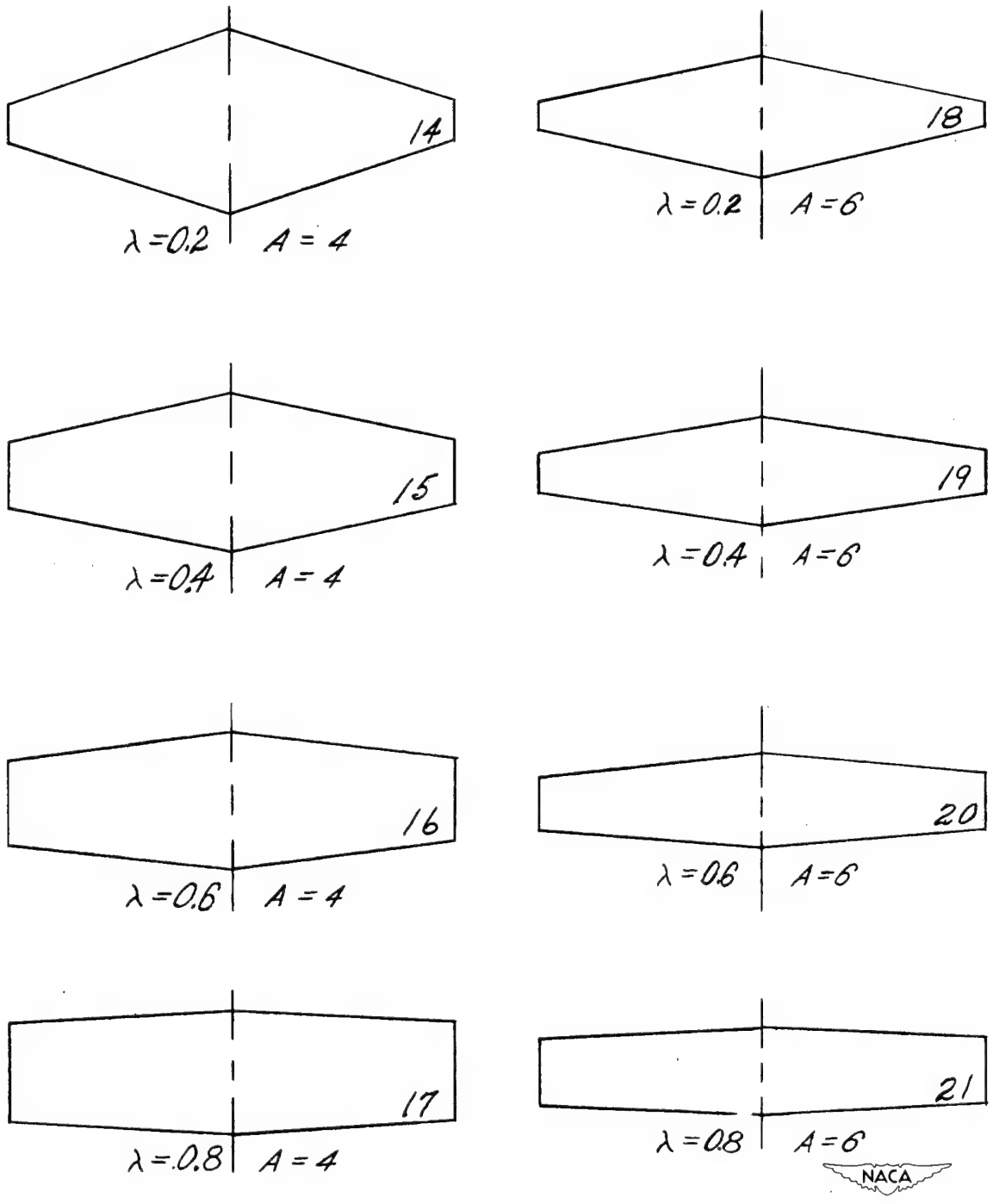

(b) Concluded.

Figure 3.– Continued.

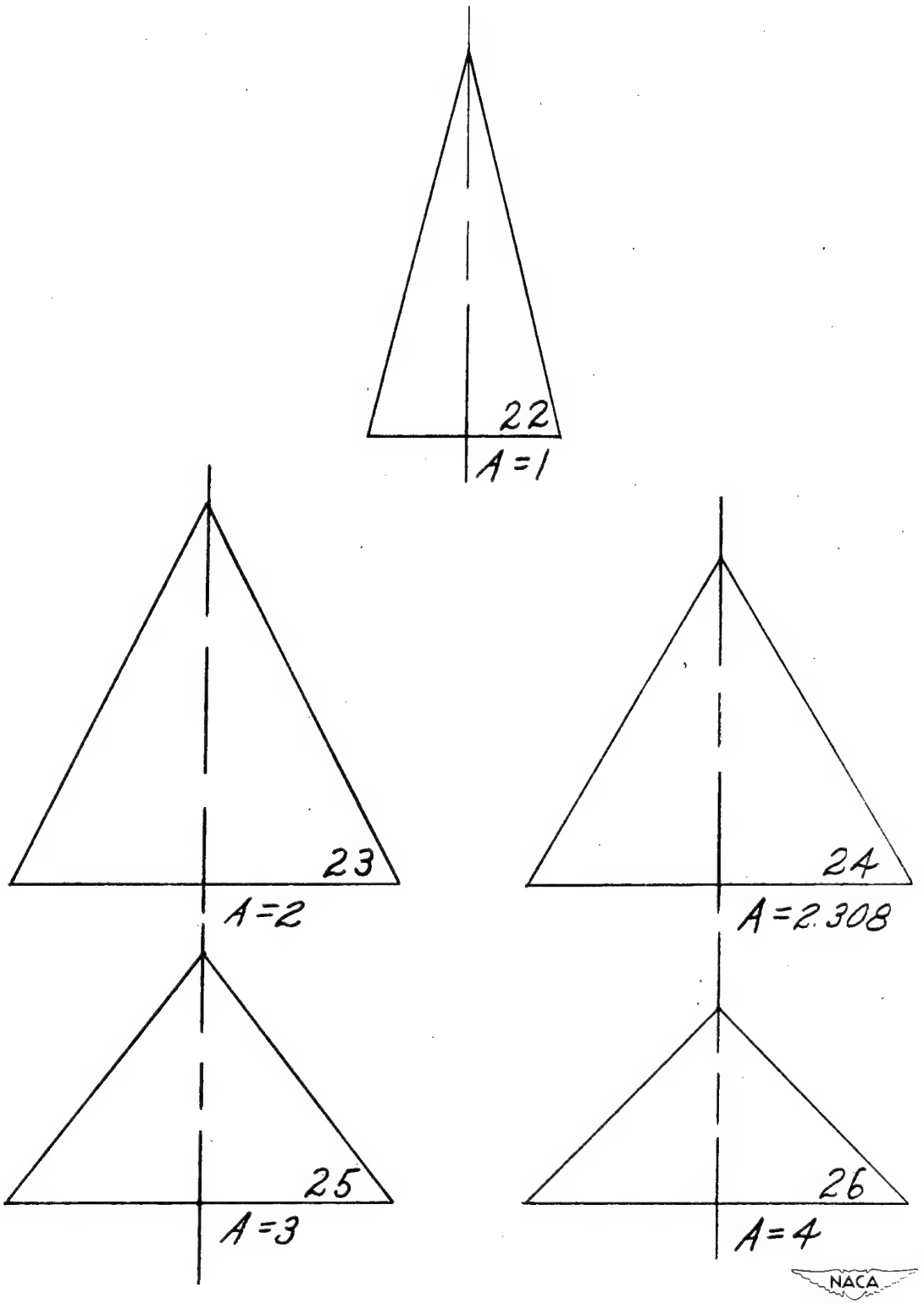

(c) Triangular wings.

Figure 3.- Continued.

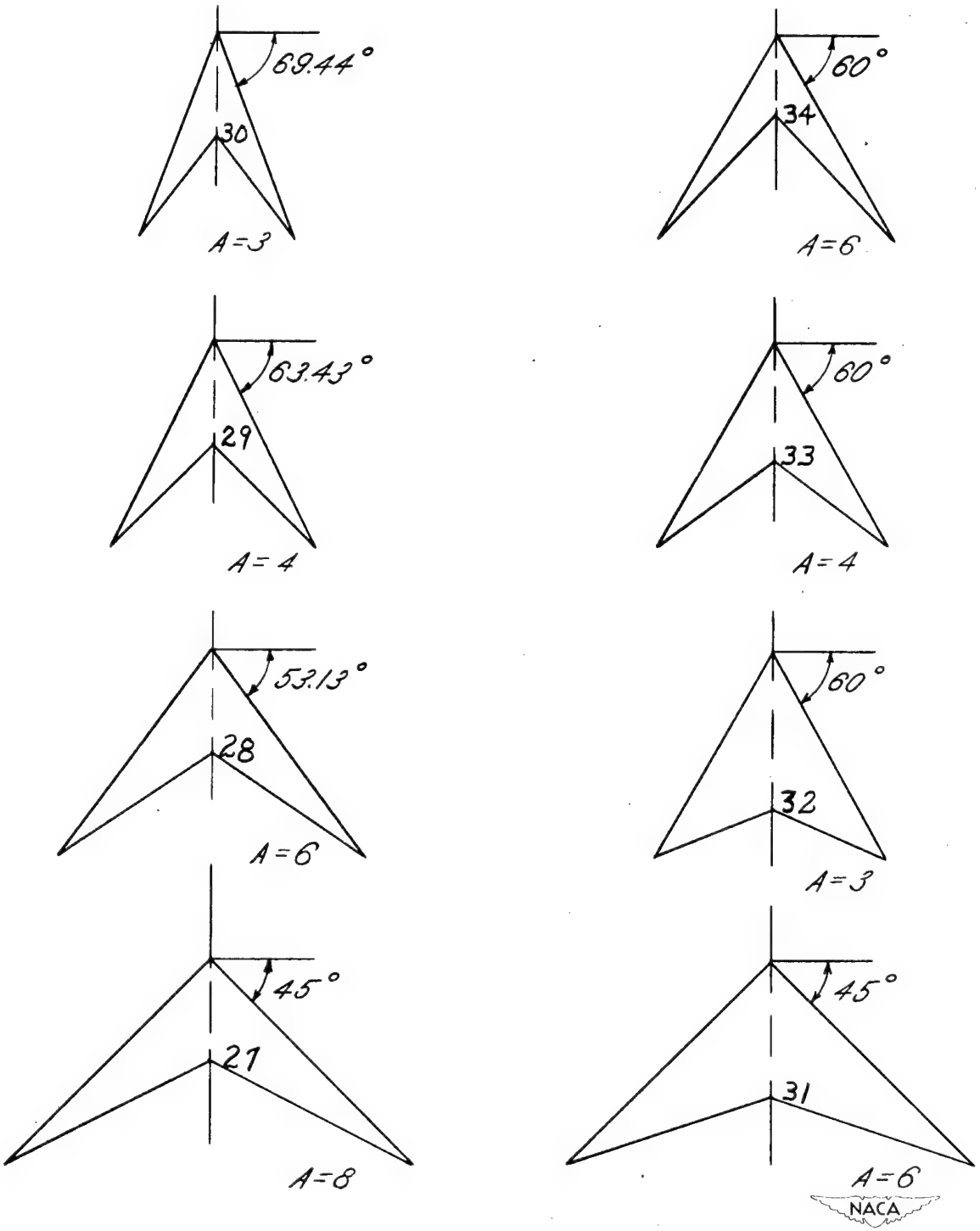

(d) Notched triangular wings.

Figure 3.- Continued.

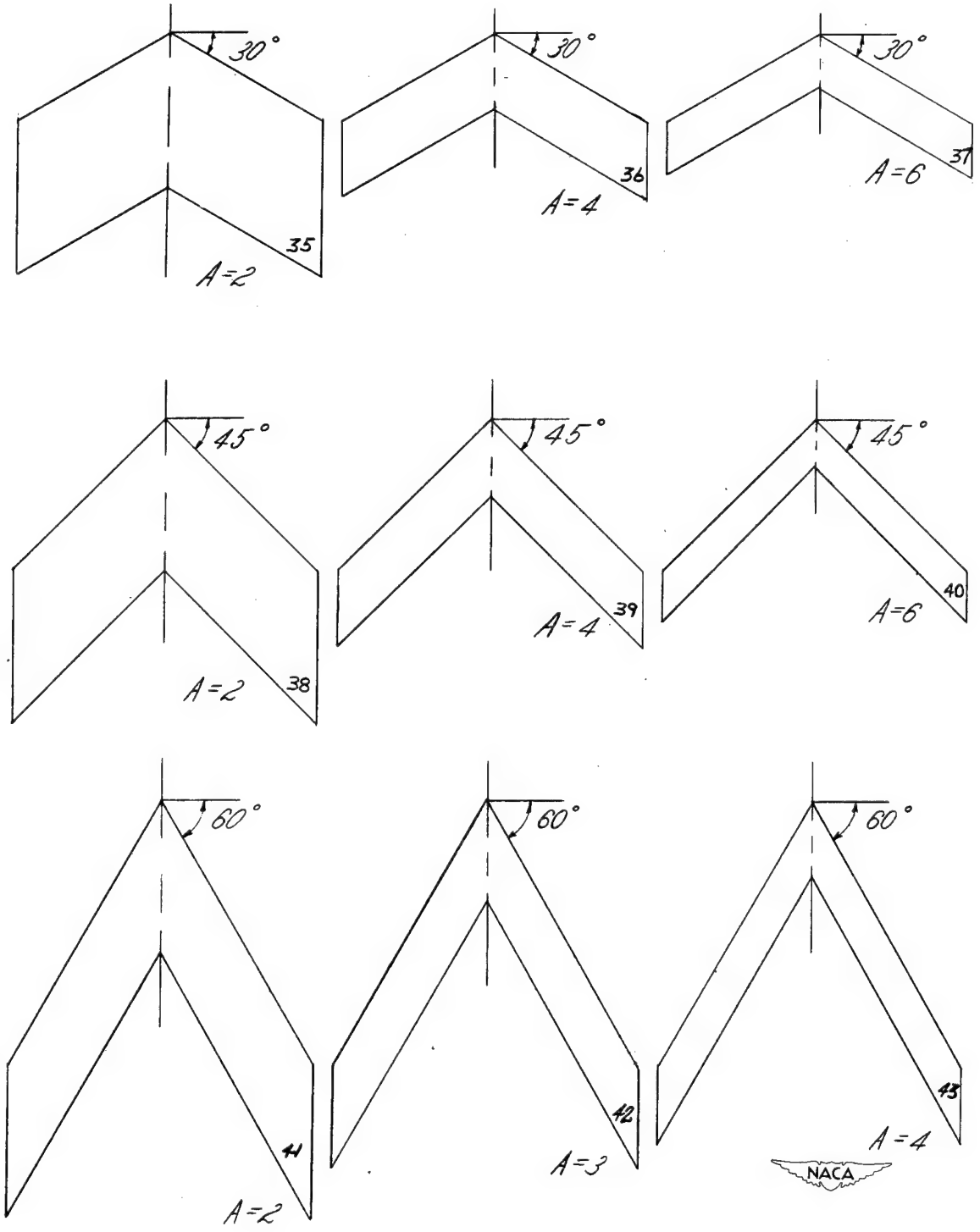

(e) Swept untapered wings.

Figure 3.– Continued.

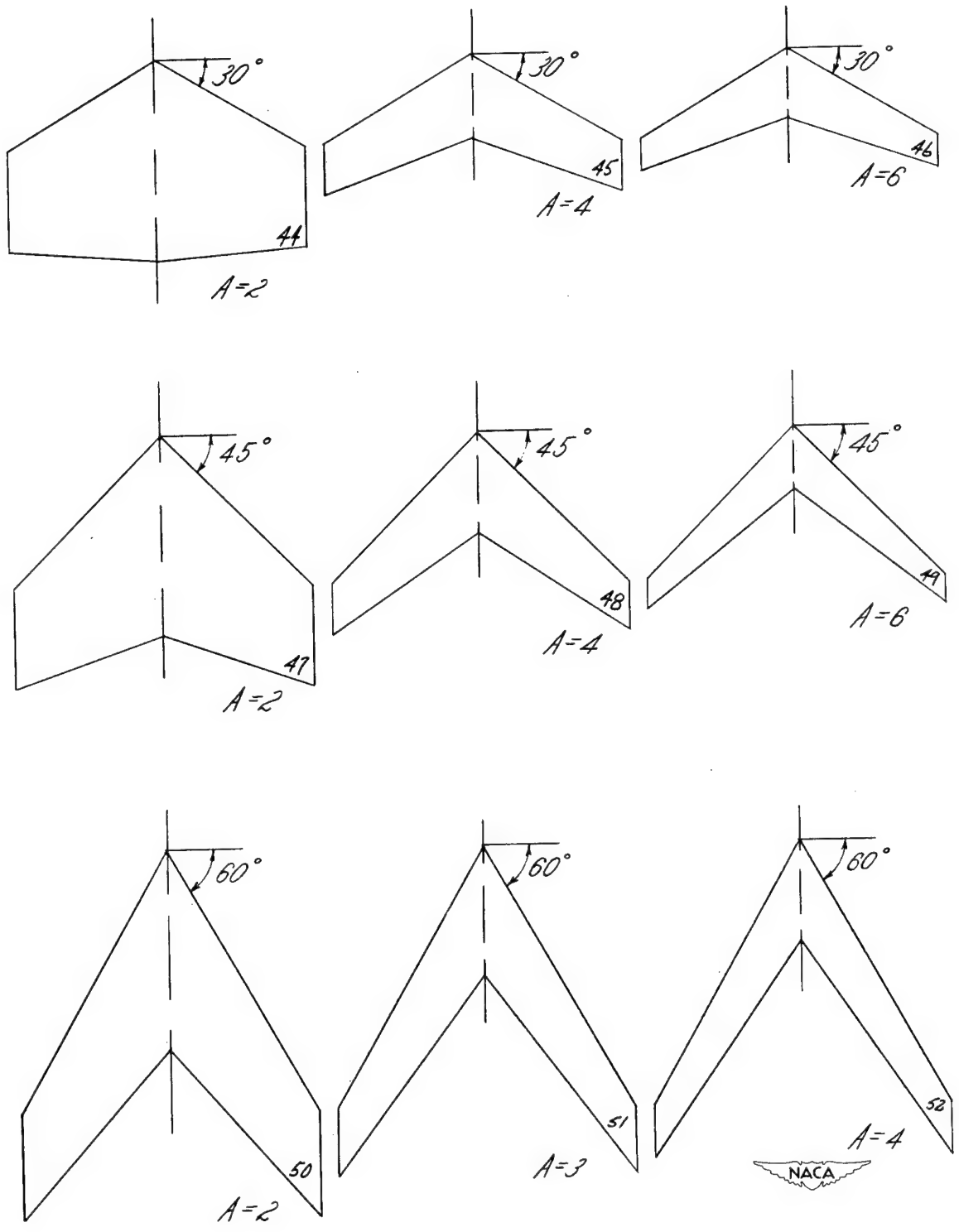

(f) Swept tapered wings; $\lambda = 0.5$.

Figure 3.- Concluded.

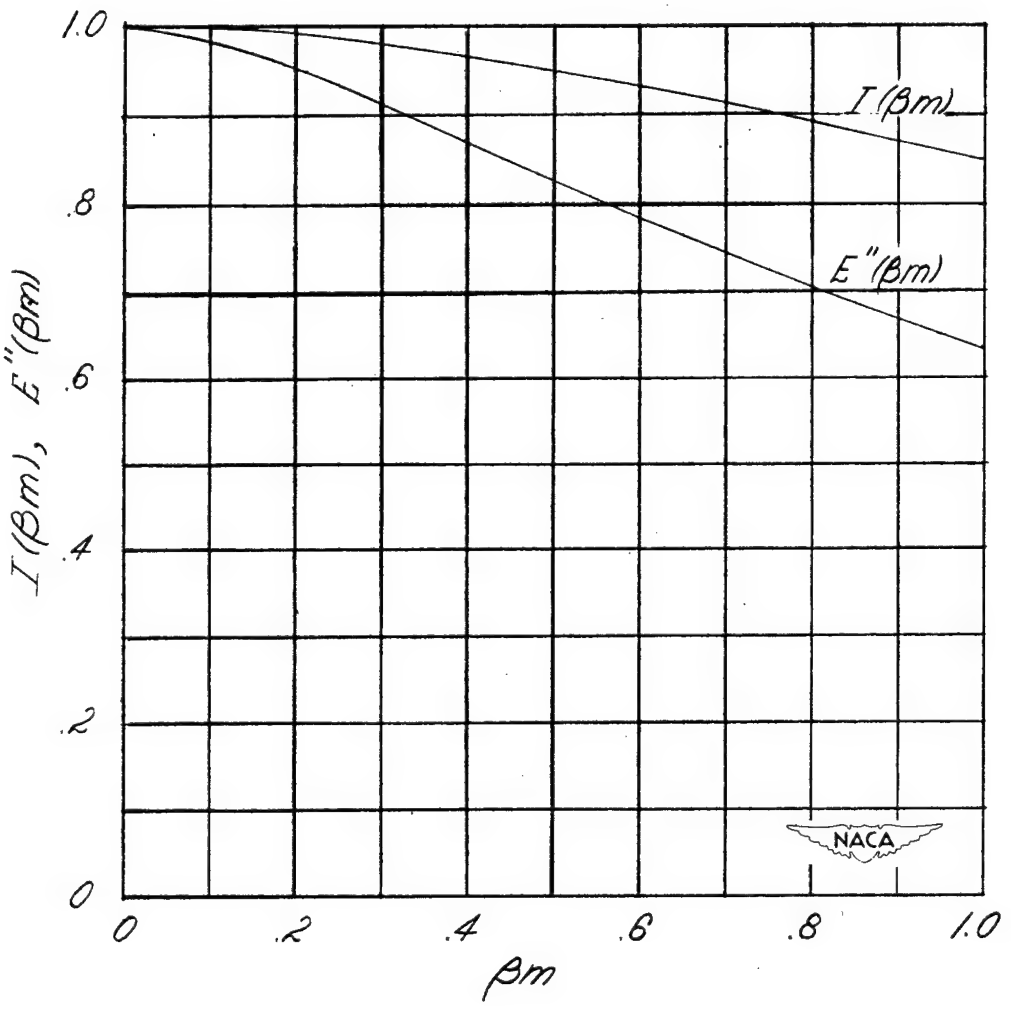

Figure 4.– Elliptic–integral factors of the stability derivatives that determine their variation with Mach number.

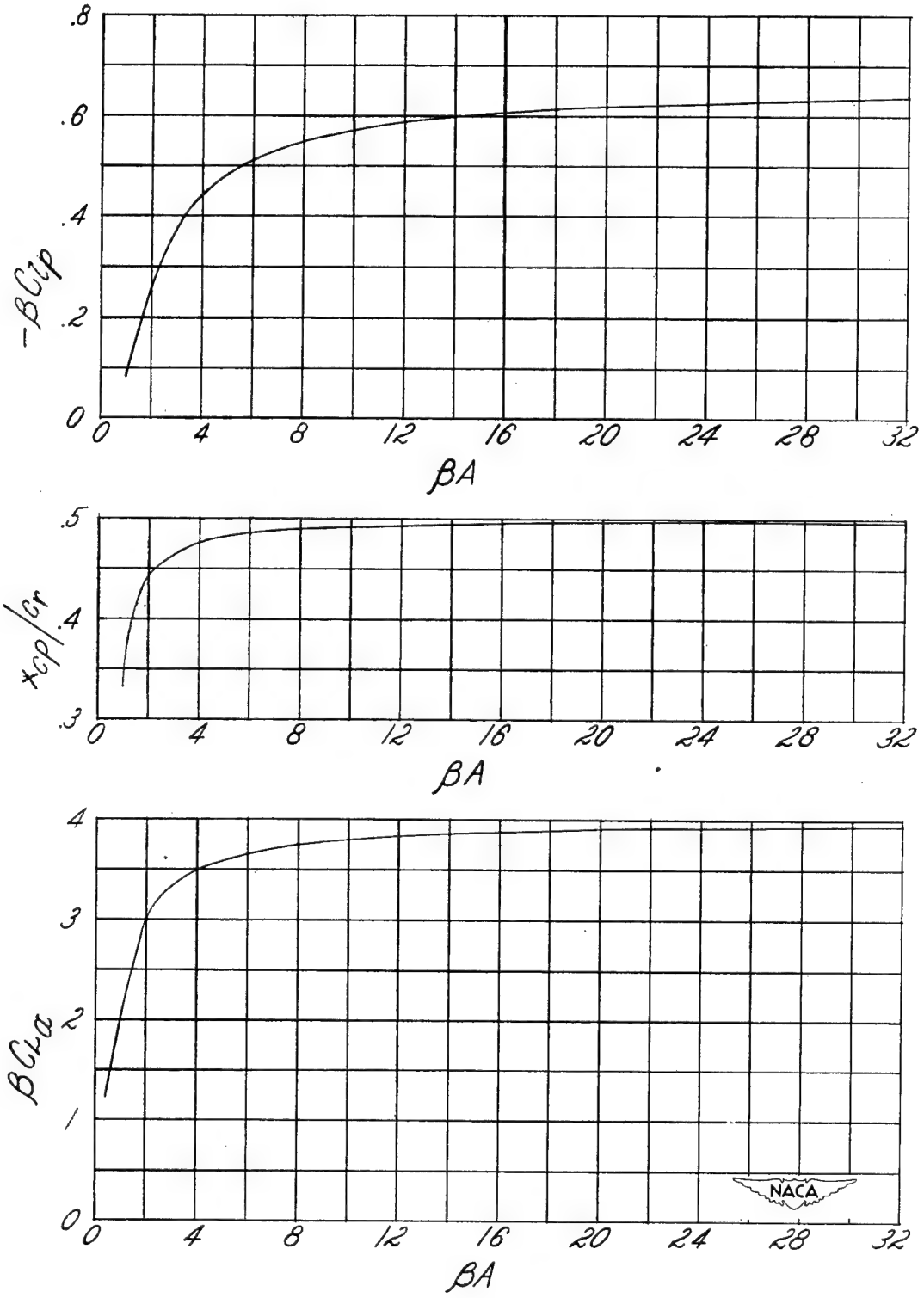

Figure 5.– Variation of βC_{L_α}, x_{cp}/c_r, and $-\beta C_{l_p}$ with βA for rectangular wings.

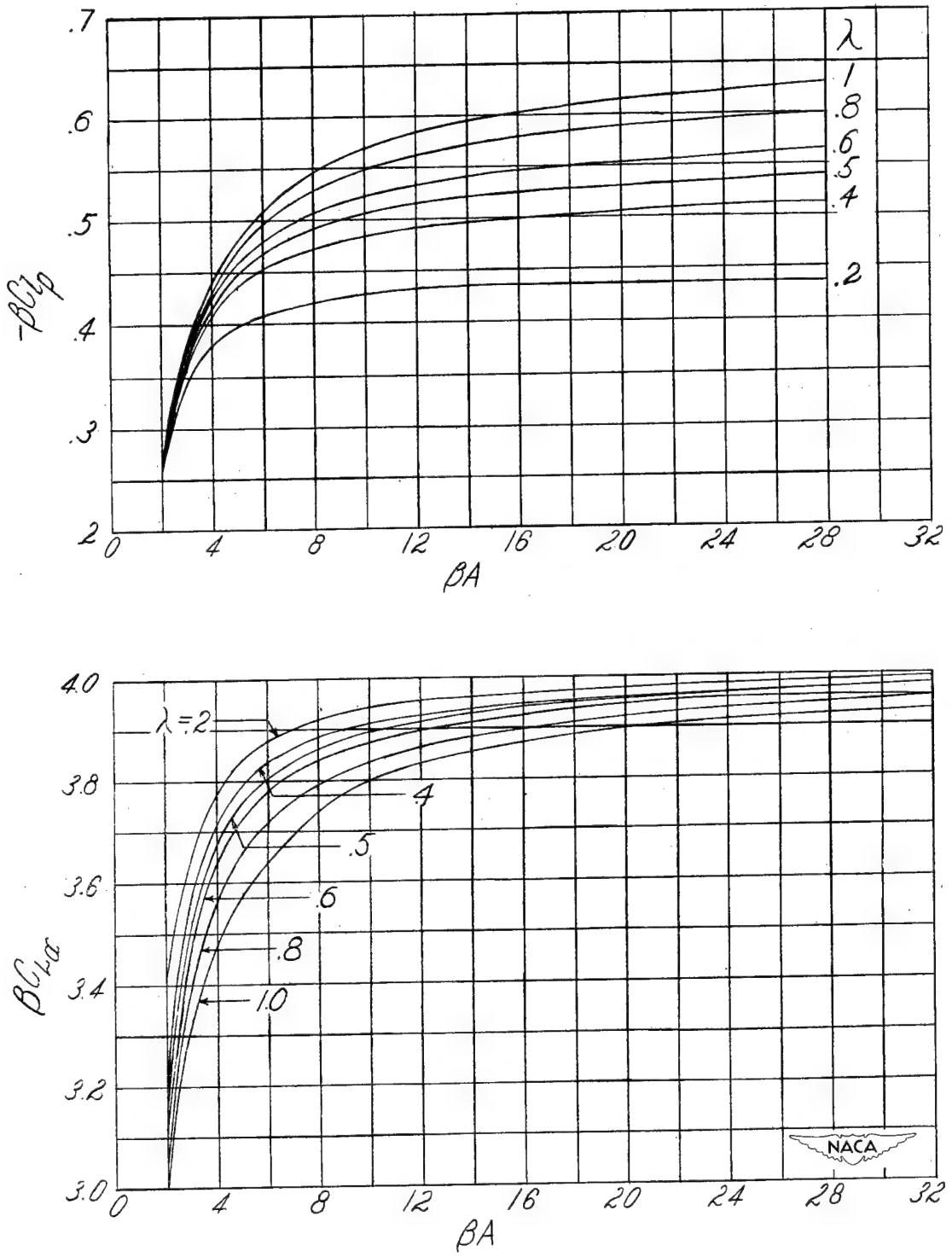

Figure 6.– Variation of βC_{L_α} and $-\beta C_{l_p}$ with βA for various taper ratios.

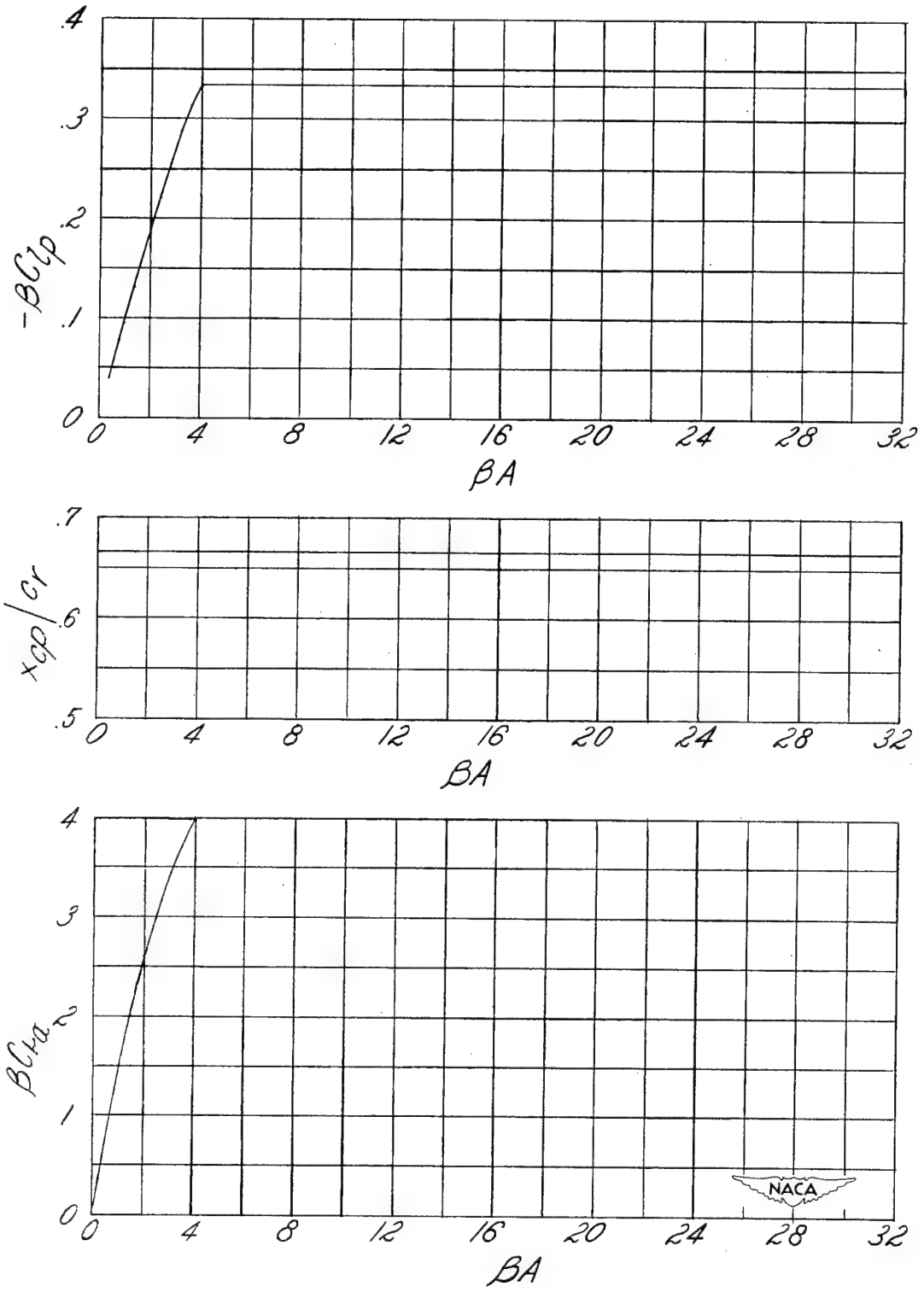

Figure 7.– Variation of βC_{L_α}, x_{cp}/c_r, and $-\beta C_{l_p}$ with βA for triangular wings.

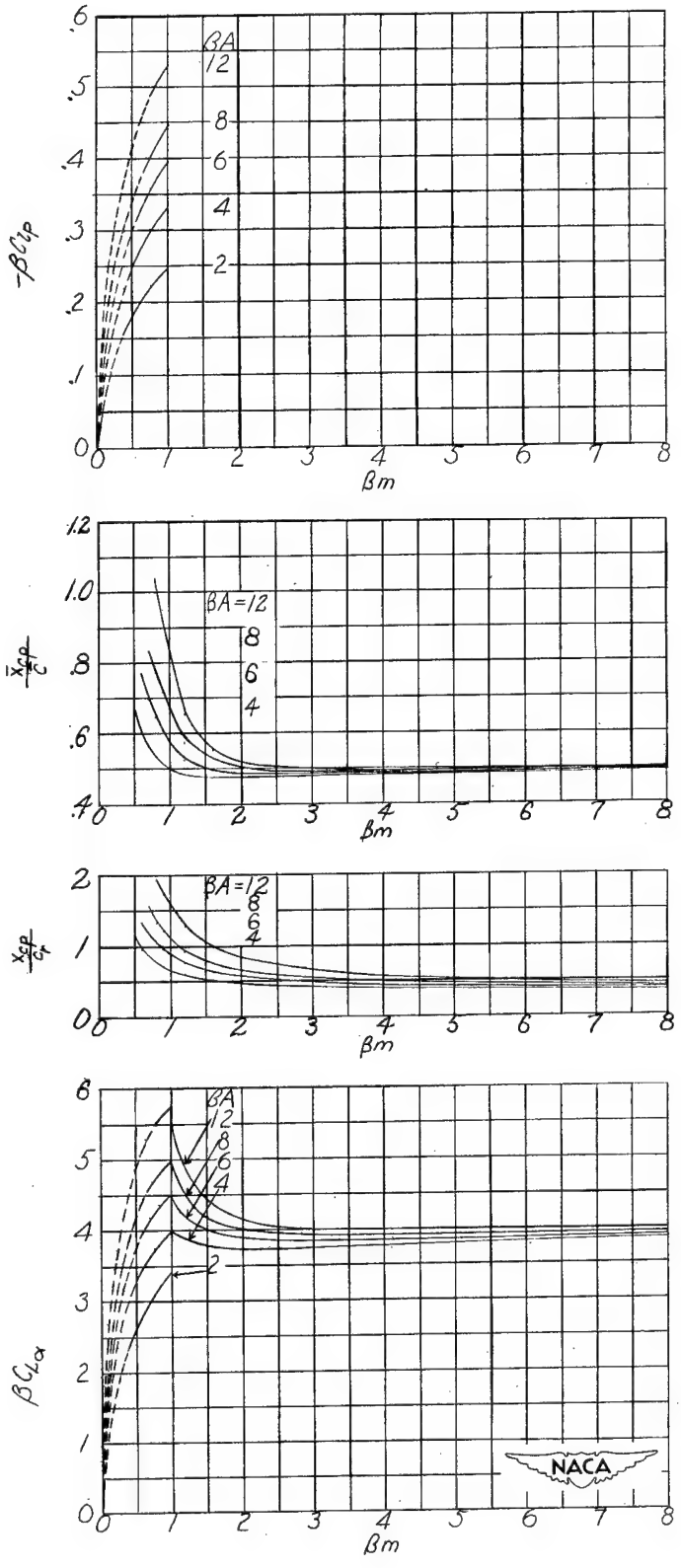

Figure 8.– Variation of βC_{L_α}, x_{cp}/c_r, $\bar{x}_{cp}/\bar{c}$, and $-\beta C_{l_p}$ with βm for notched triangular wings.

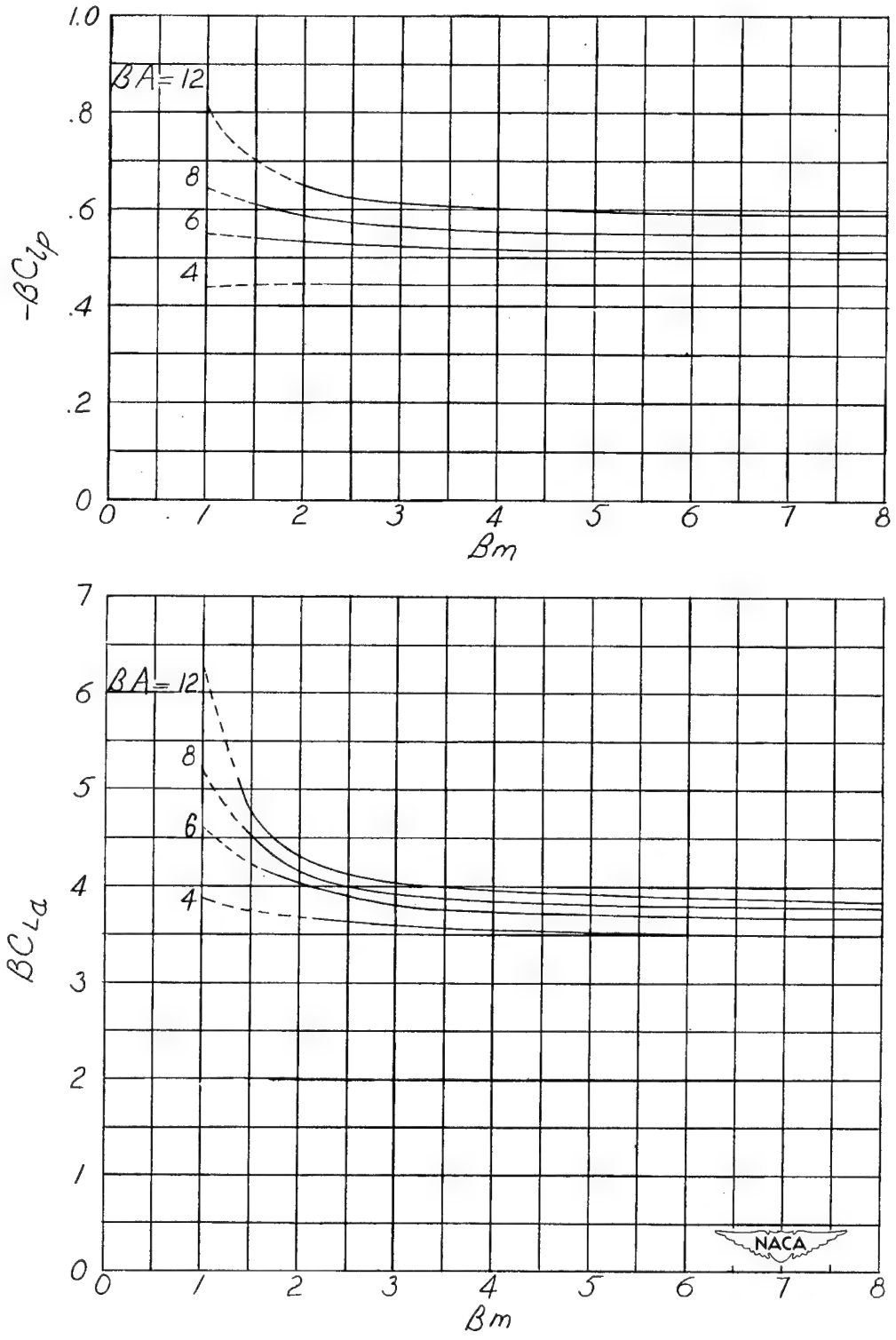

Figure 9.– Variation of βC_{L_α} and $-\beta C_{l_p}$ with βm for swept untapered wings with supersonic leading edges.

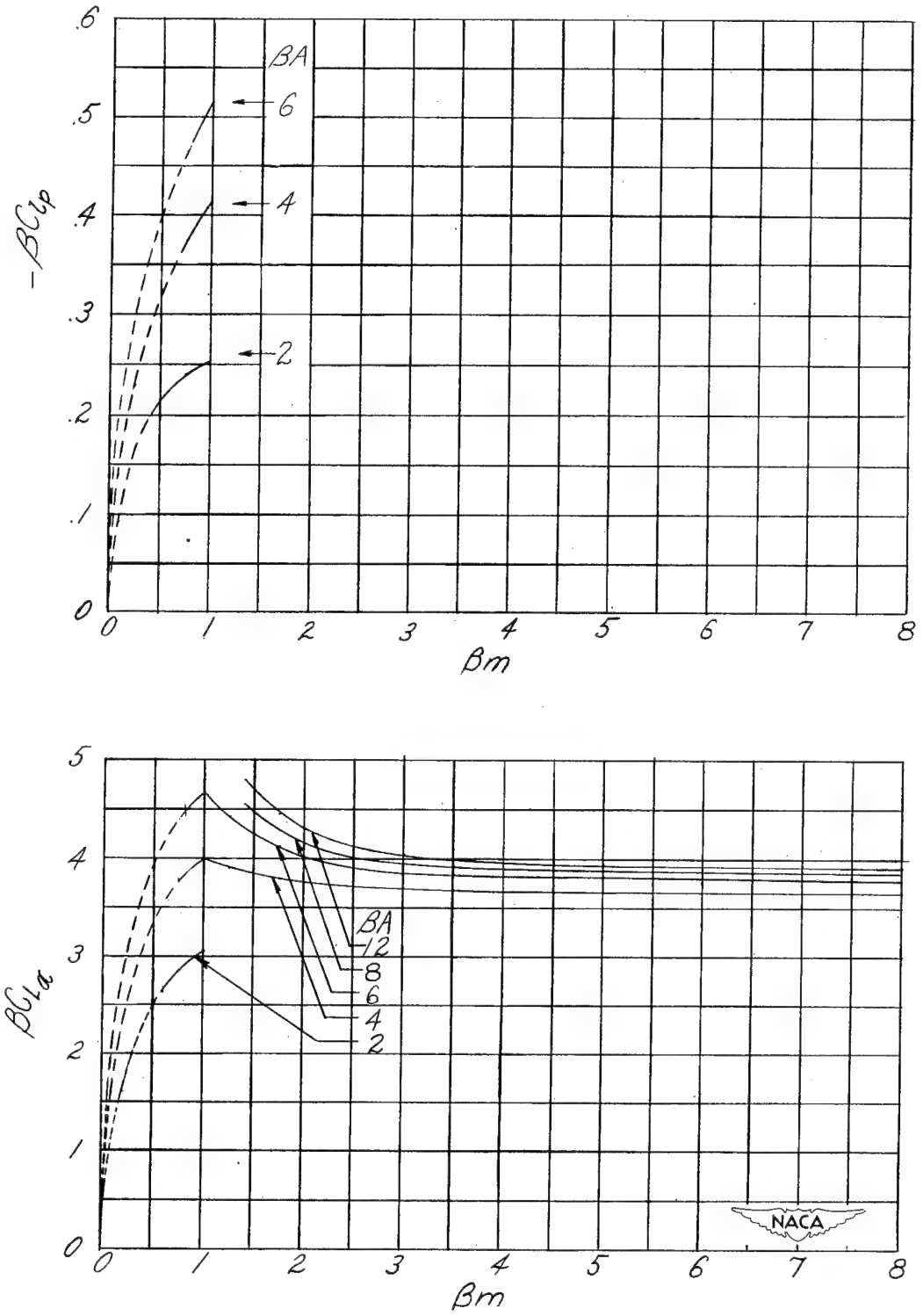

Figure 10.– Variation of βC_{L_α} and $-\beta C_{l_p}$ with βm for swept tapered wings. Taper ratio, 0.5.

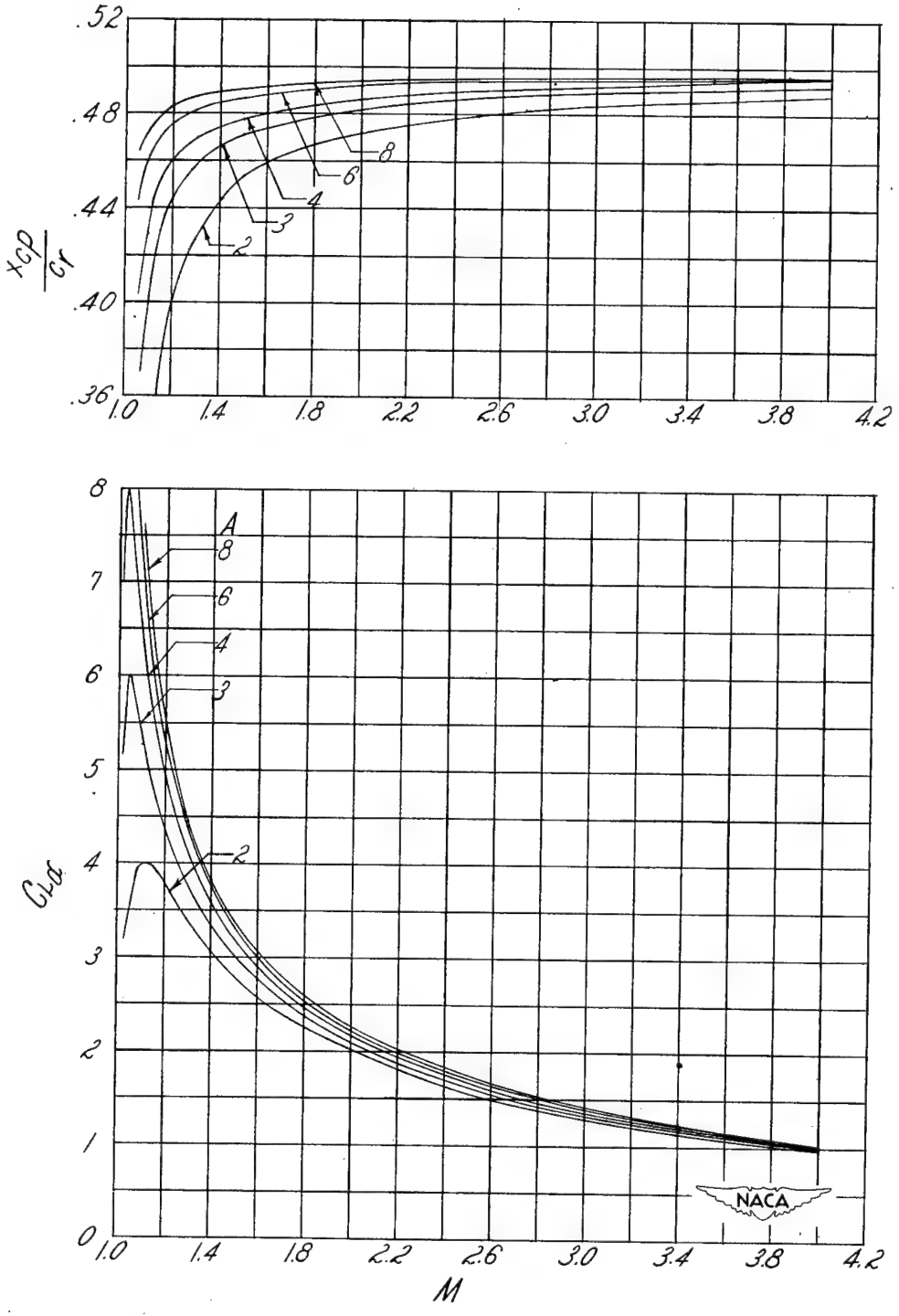

(a) Variation of C_{L_α} and x_{cp}/c_r with Mach number.

Figure 11.– Variation of C_{L_α}, x_{cp}/c_r, and $-C_{l_p}$ with Mach number for rectangular wings of aspect ratio 2, 3, 4, 6, and 8.

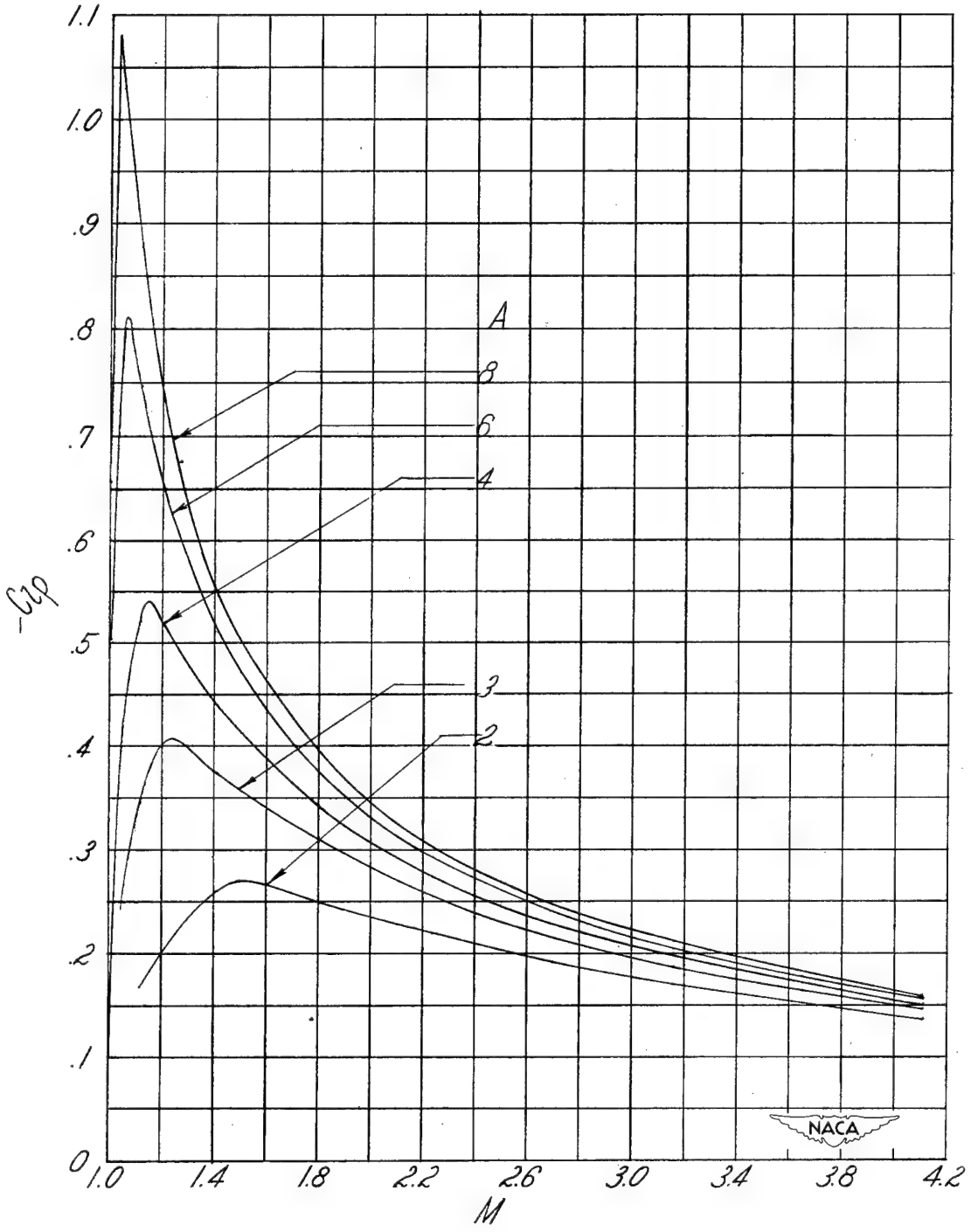

(b) Variation of $-C_{l_p}$ with Mach number.

Figure 11.– Concluded.

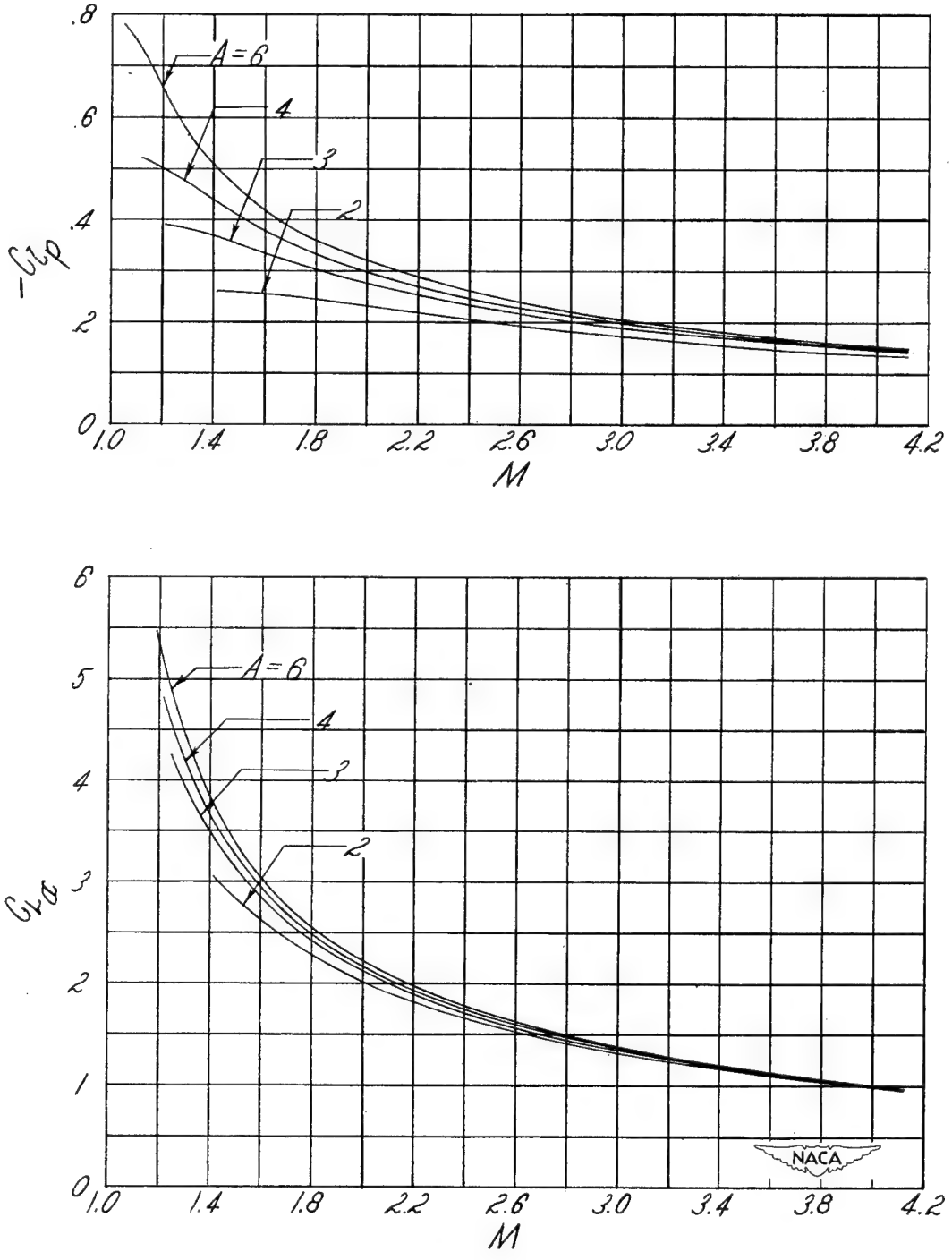

(a) Taper ratio, 0.8.

Figure 12.– Variation of C_{L_α} and $-C_{l_p}$ with Mach number for unswept tapered wings.

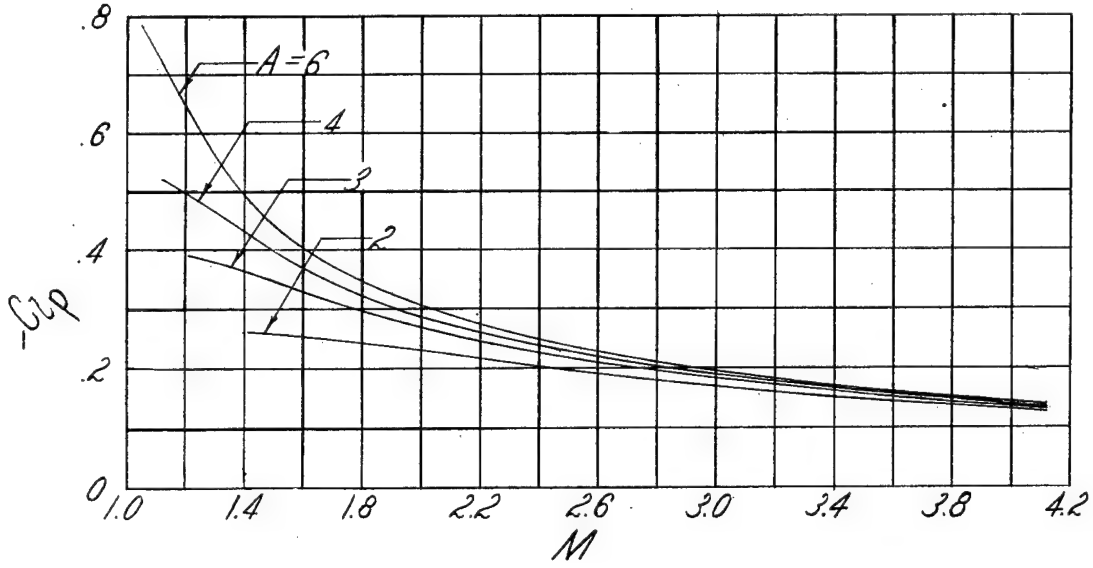

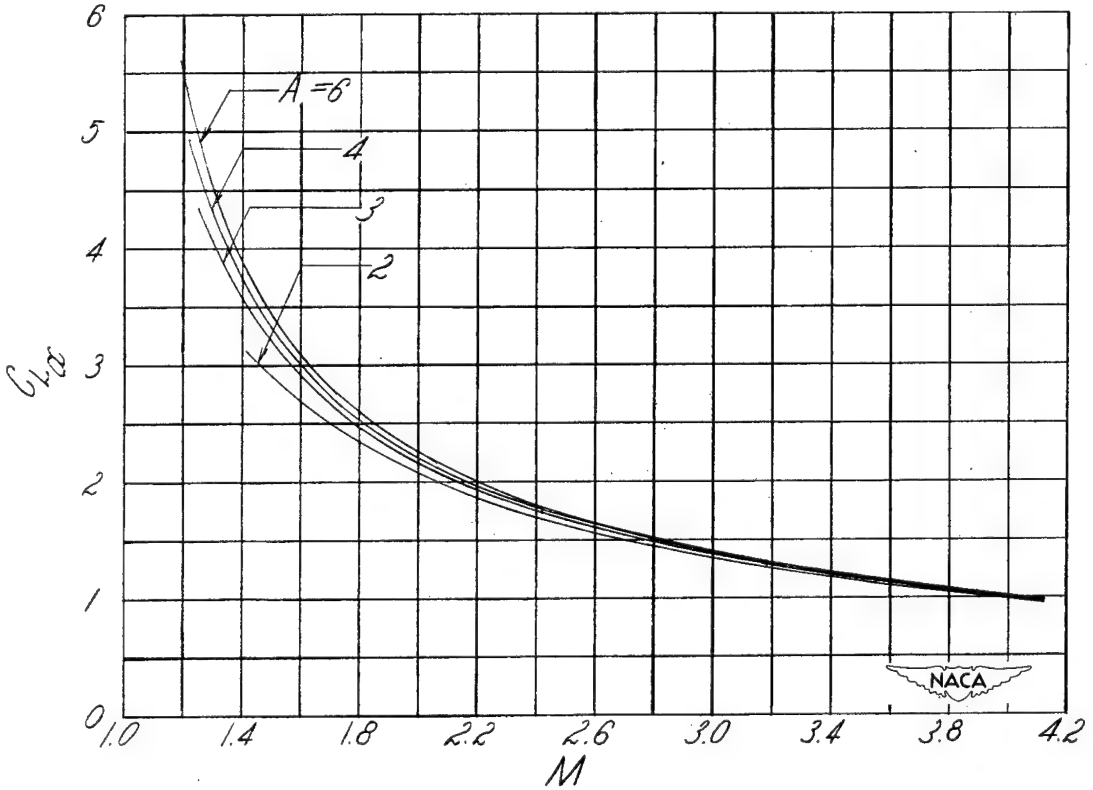

(b) Taper ratio, 0.6.

Figure 12.- Continued.

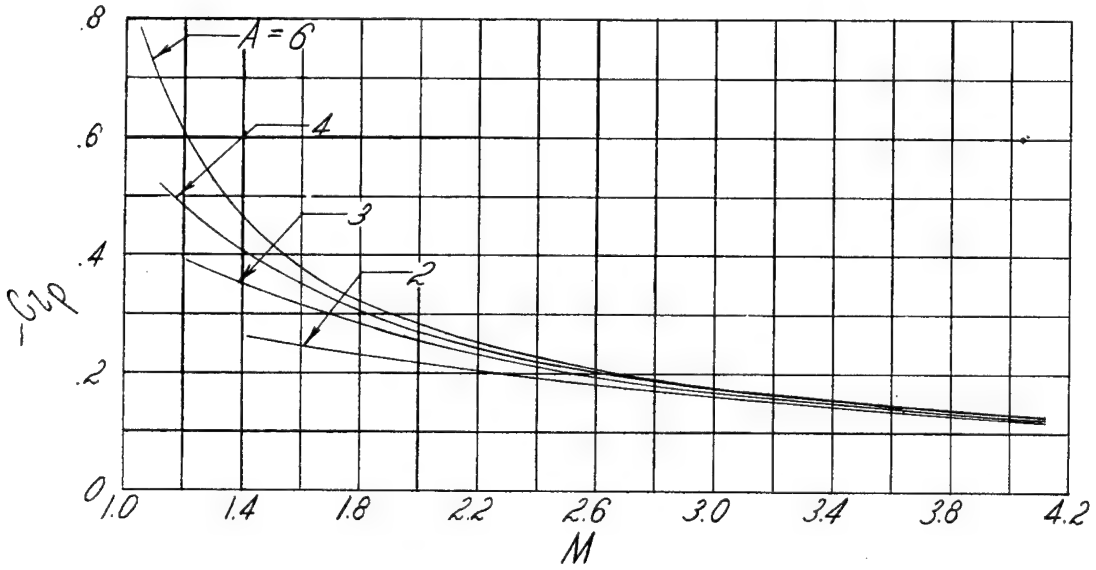

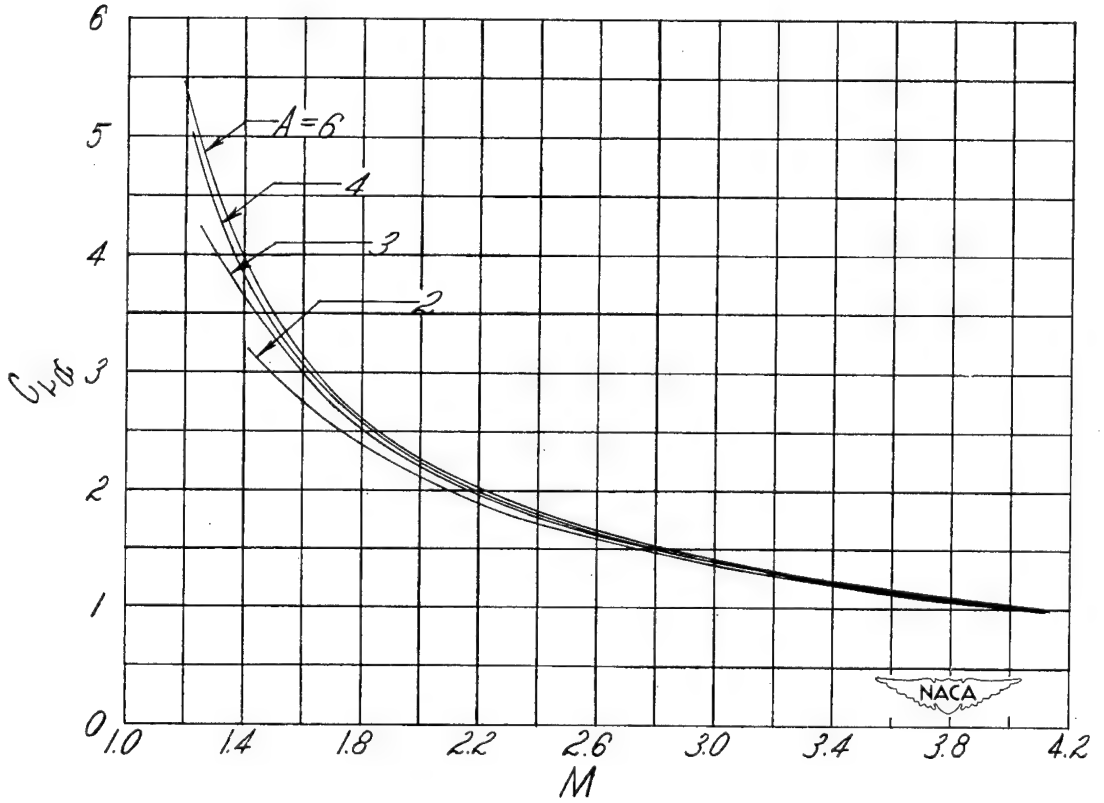

(c) Taper ratio, 0.4.

Figure 12.– Continued.

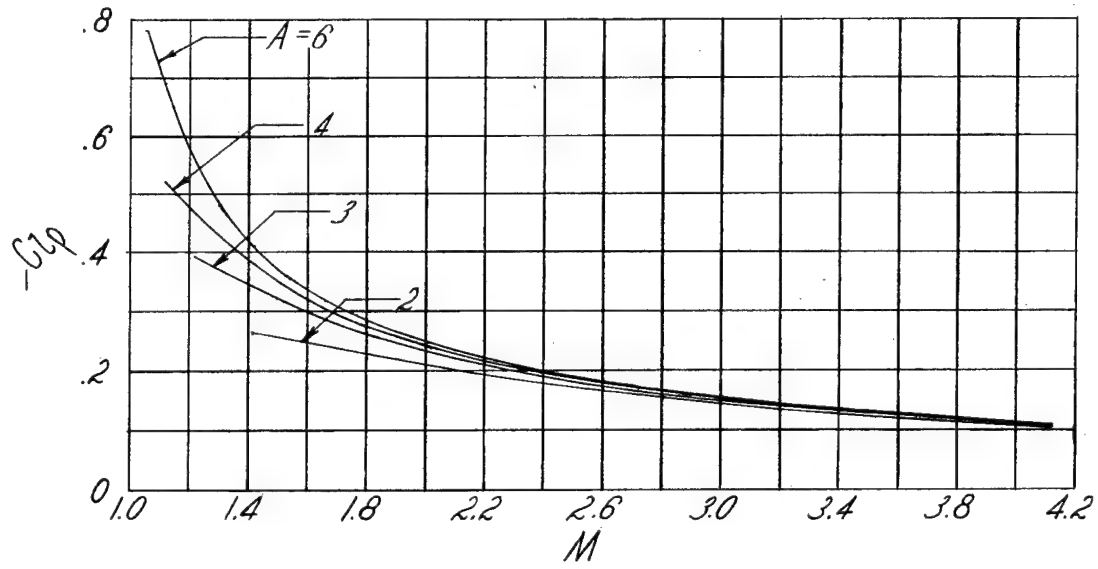

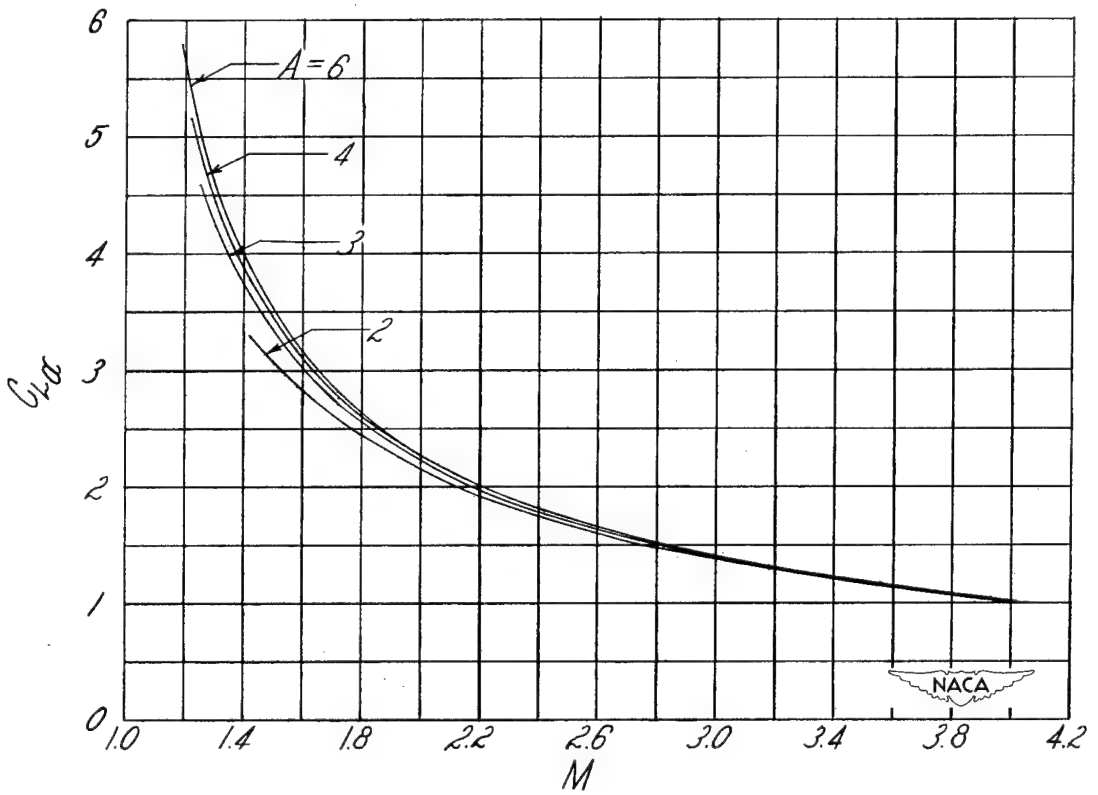

(d) Taper ratio, 0.2.

Figure 12.– Concluded.

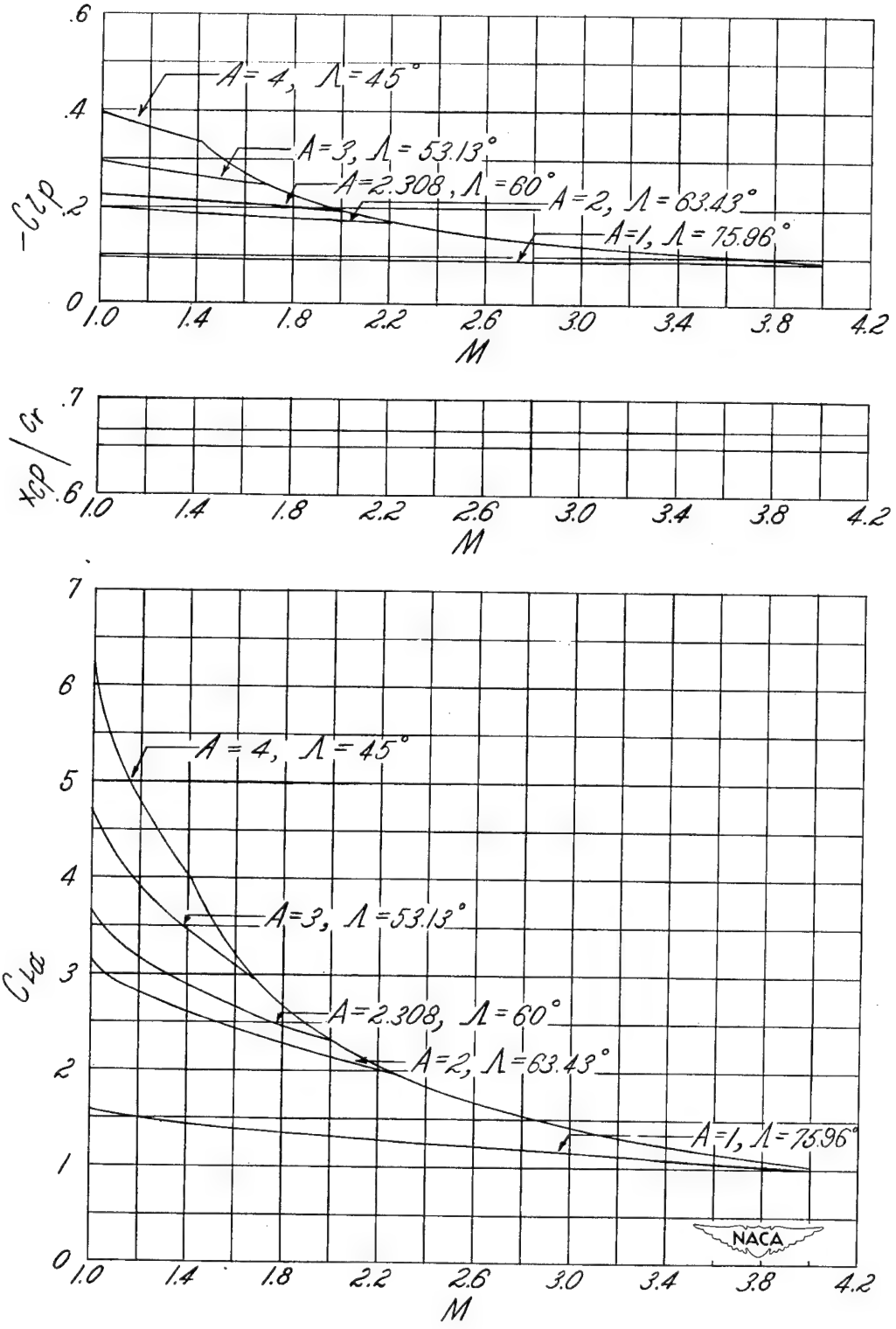

Figure 13.– Variation of C_{L_α}, x_{cp}/c_r, and $-C_{l_p}$ with Mach number for triangular wings.

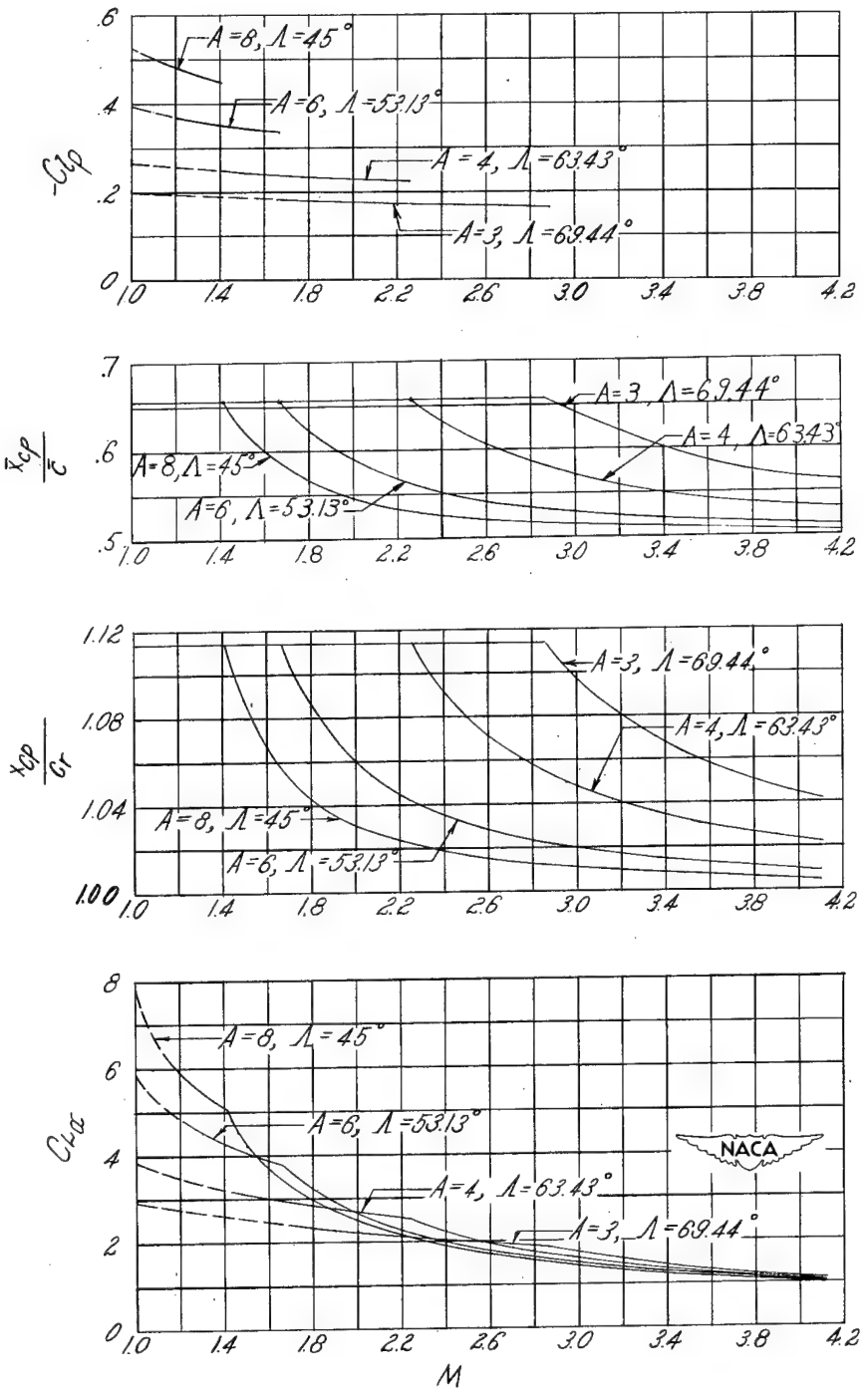

(a) $N = 1 - 4 \cot \frac{\Lambda}{A} = \frac{1}{2}$.

Figure 14.– Variation of C_{L_α}, x_{cp}/c_r, $\bar{x}_{cp}/\bar{c}$, and $-C_{l_p}$ with Mach number for notched triangular wings.

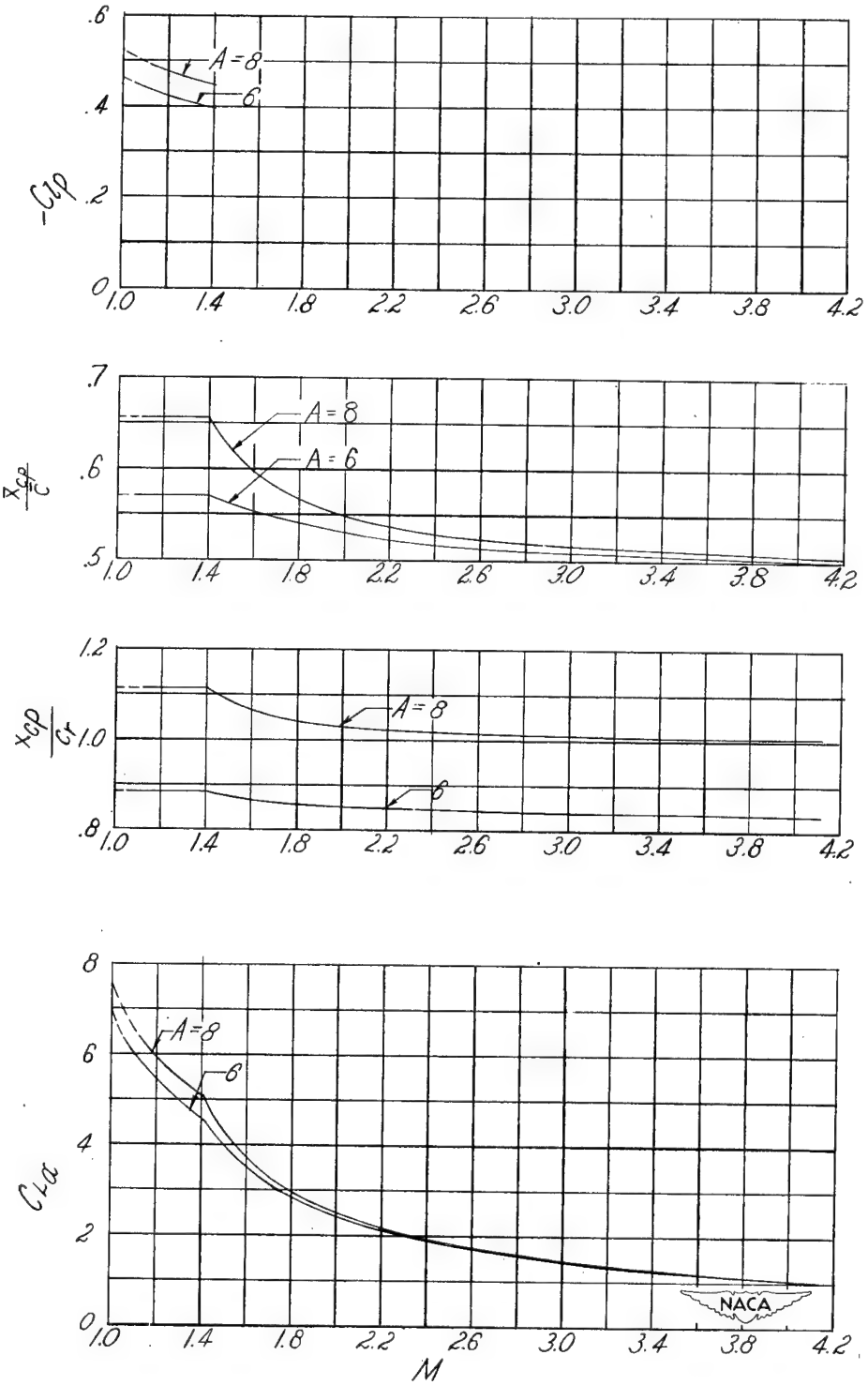

(b) Angle of sweep, 45°.

Figure 14.– Continued.

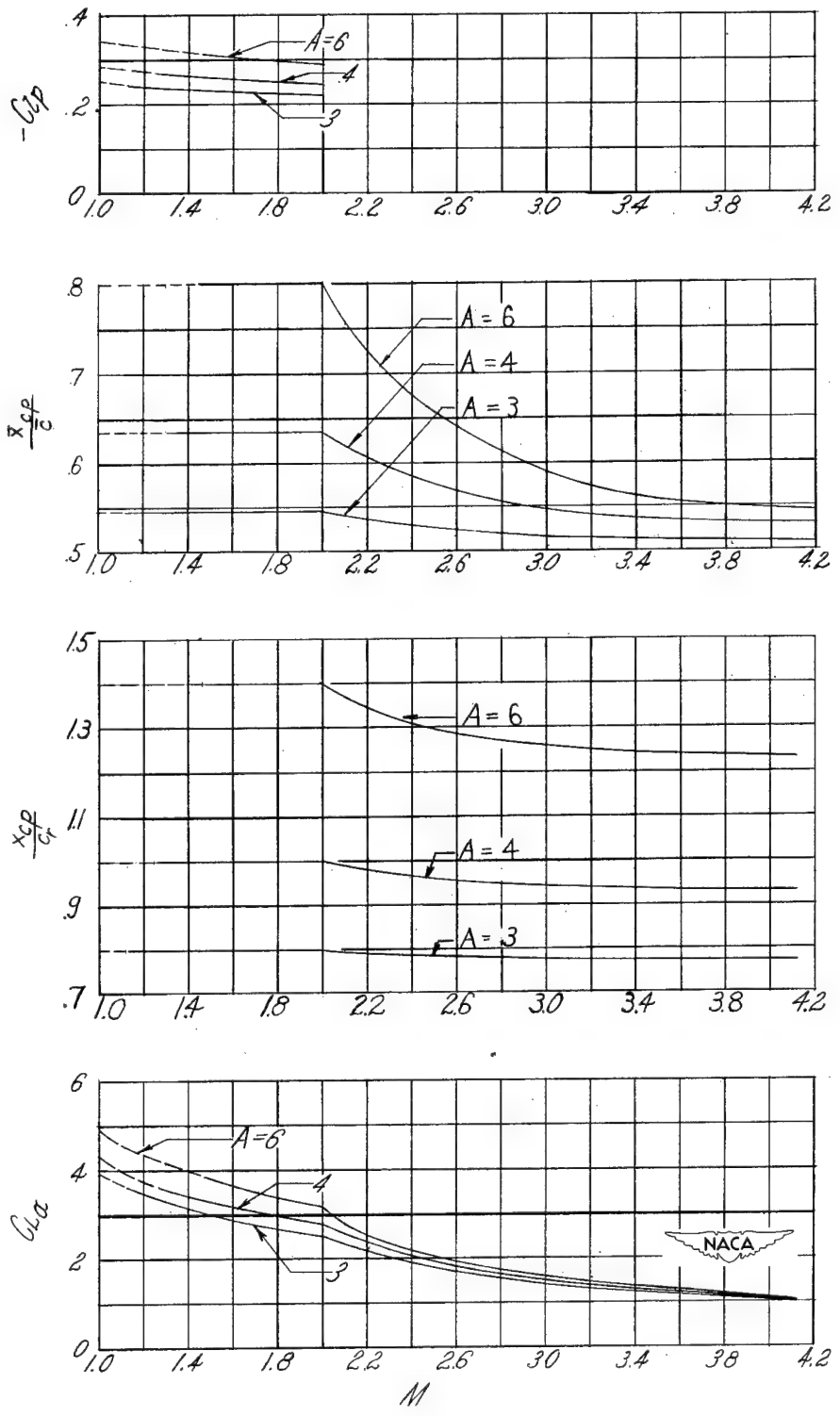

(c) Angle of sweep, 60°.

Figure 14.– Concluded.

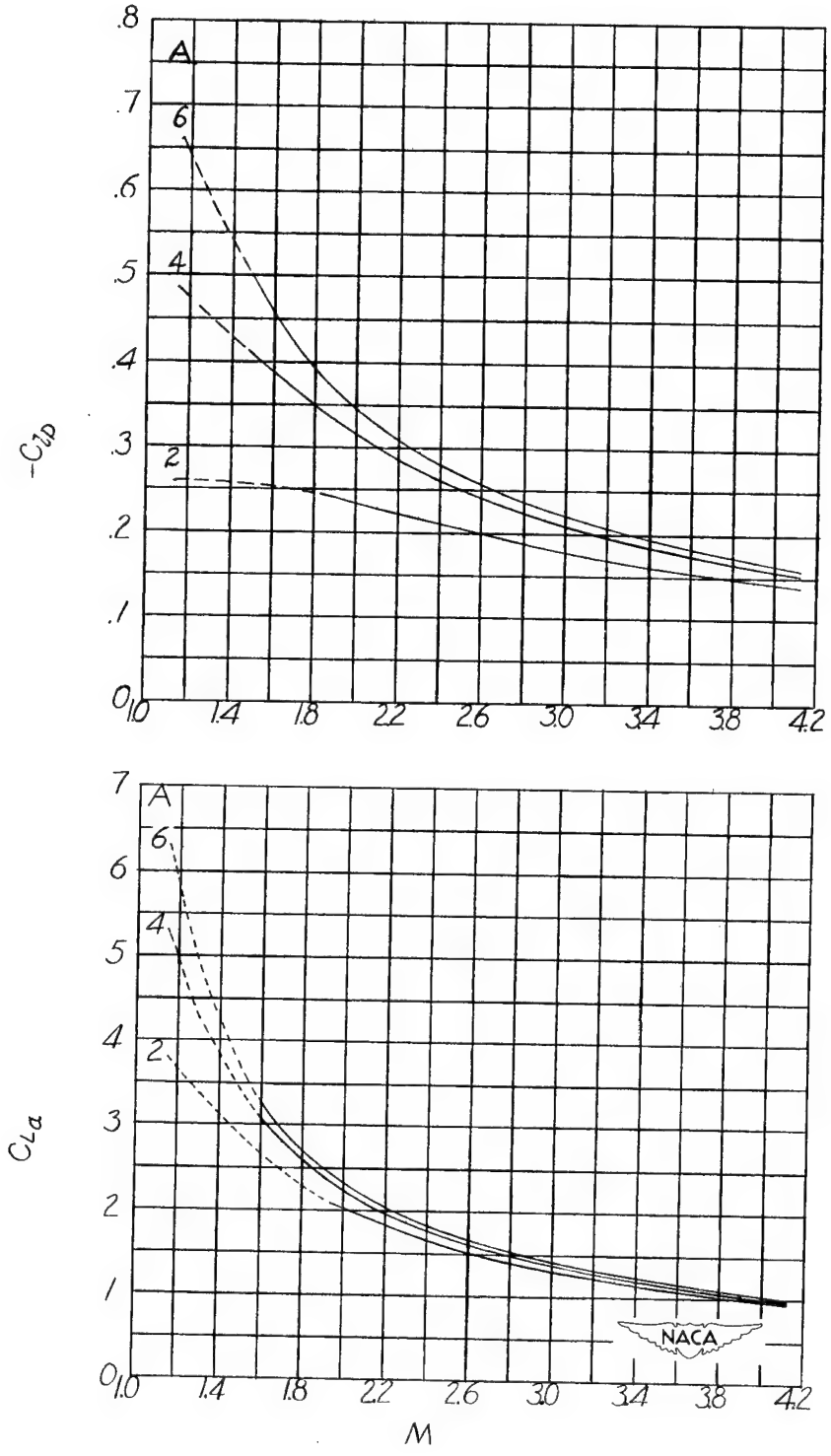

(a) Angle of sweep, 30°.

Figure 15.– Variation of C_{L_α} and $-C_{l_p}$ with Mach number for swept untapered wings.

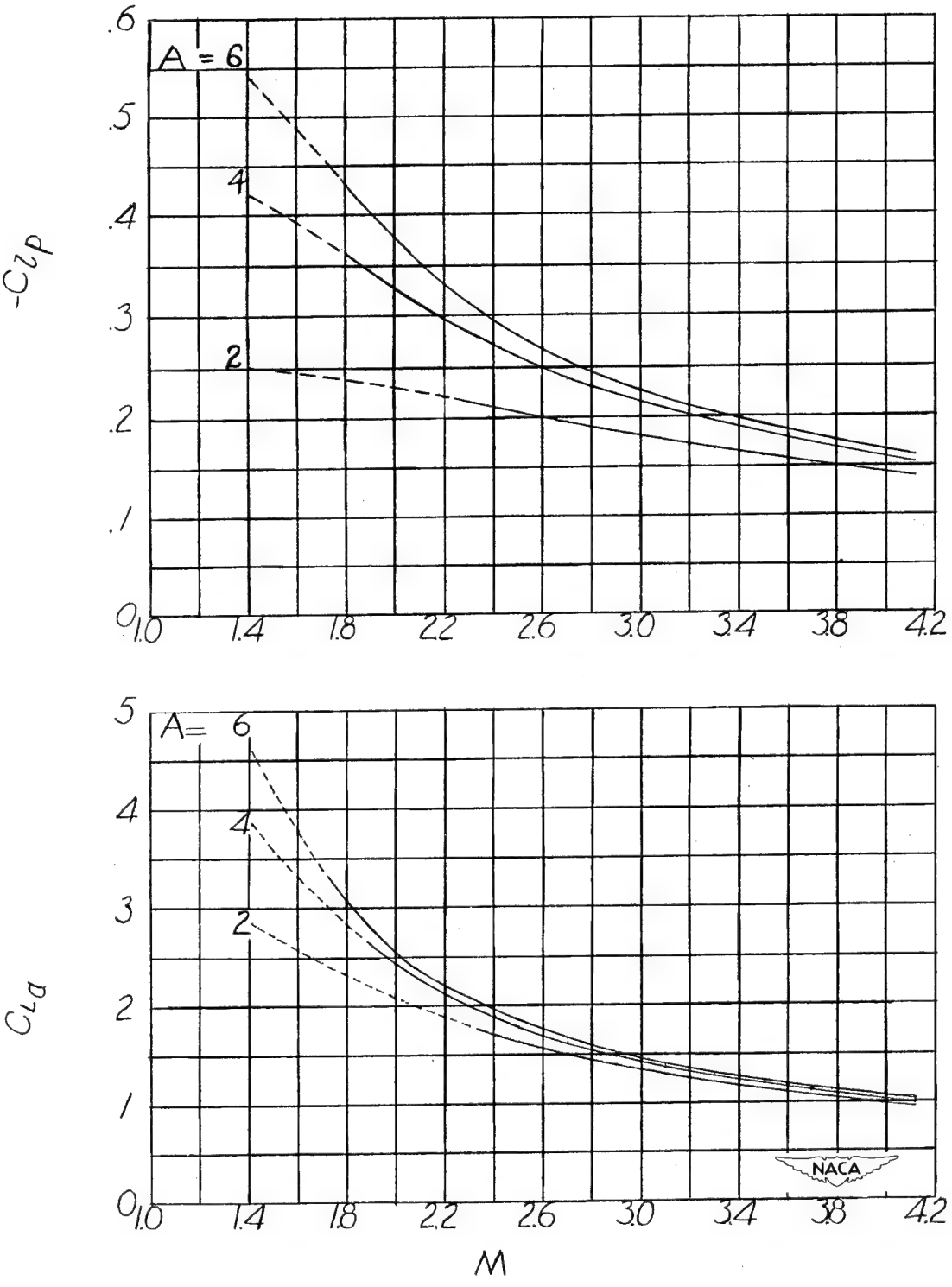

(b) Angle of sweep, 45°.

Figure 15.- Continued.

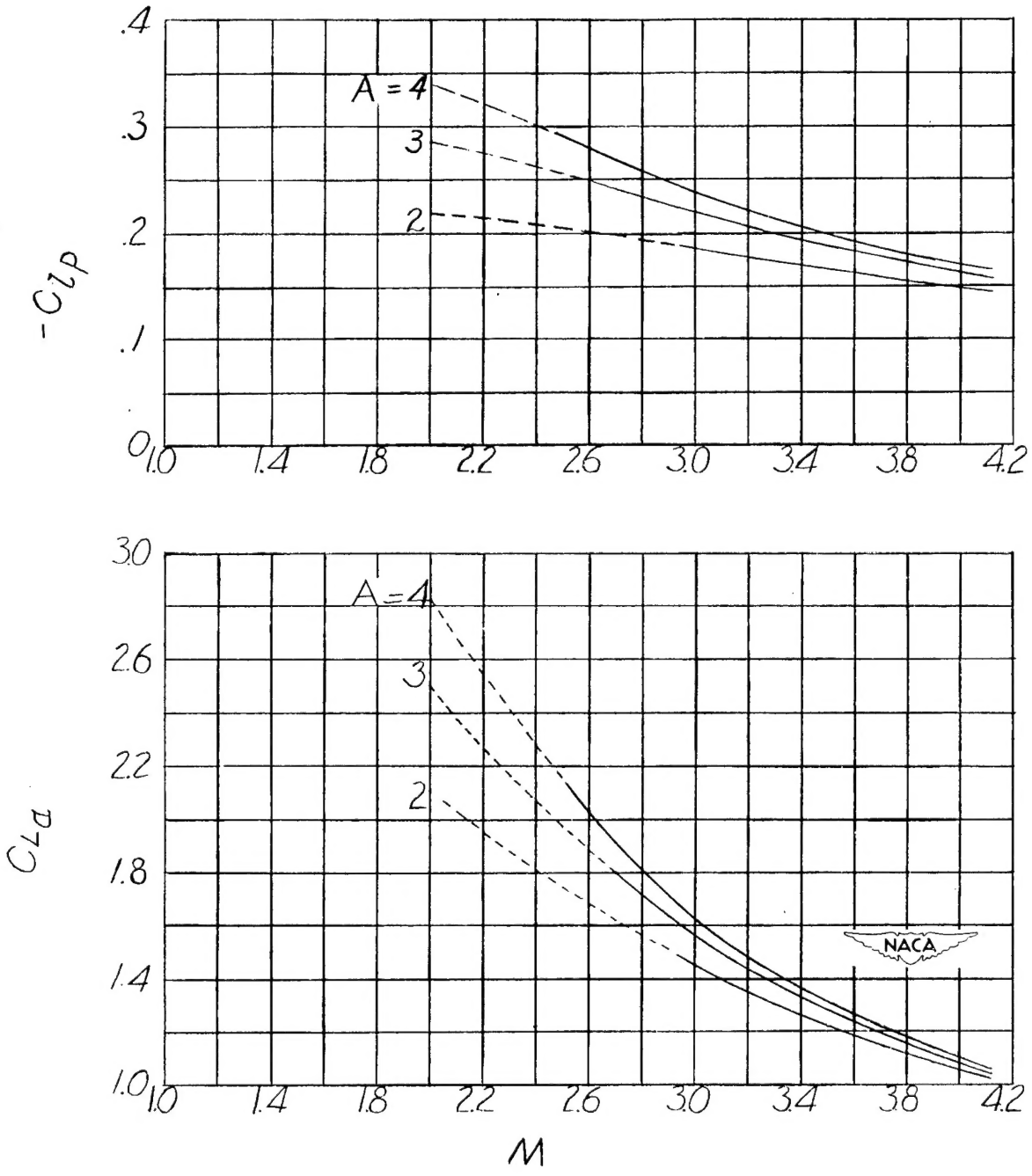

(c) Angle of sweep, 60°.

Figure 15.– Concluded.

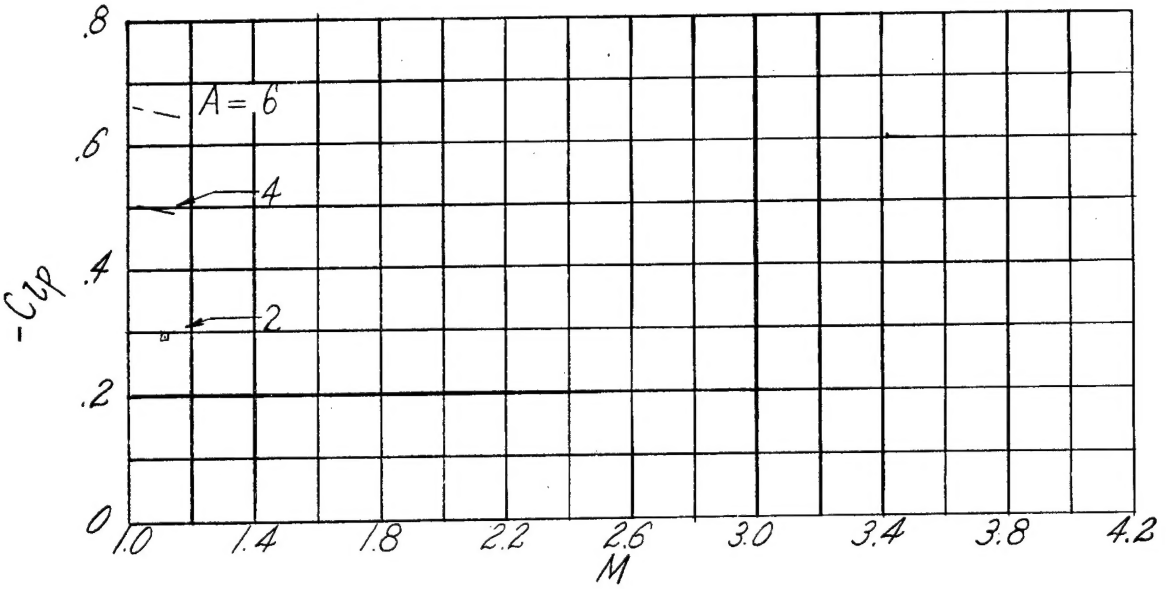

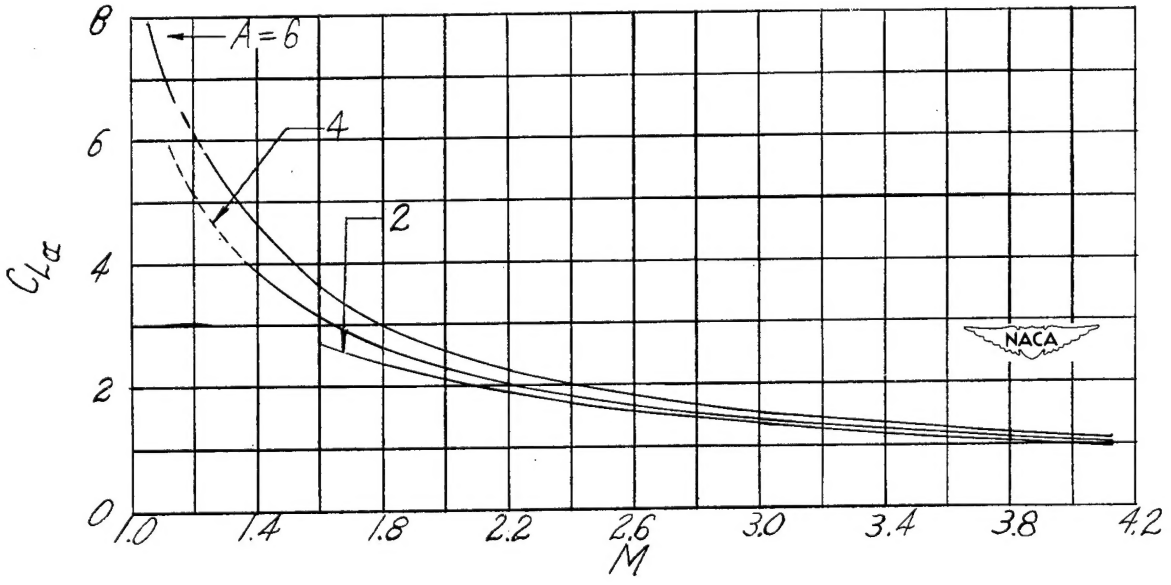

(a) Angle of sweep, 30°.

Figure 16.- Variation of C_{L_α} and $-C_{l_p}$ with Mach number for swept tapered wings. Taper ratio, 0.5.

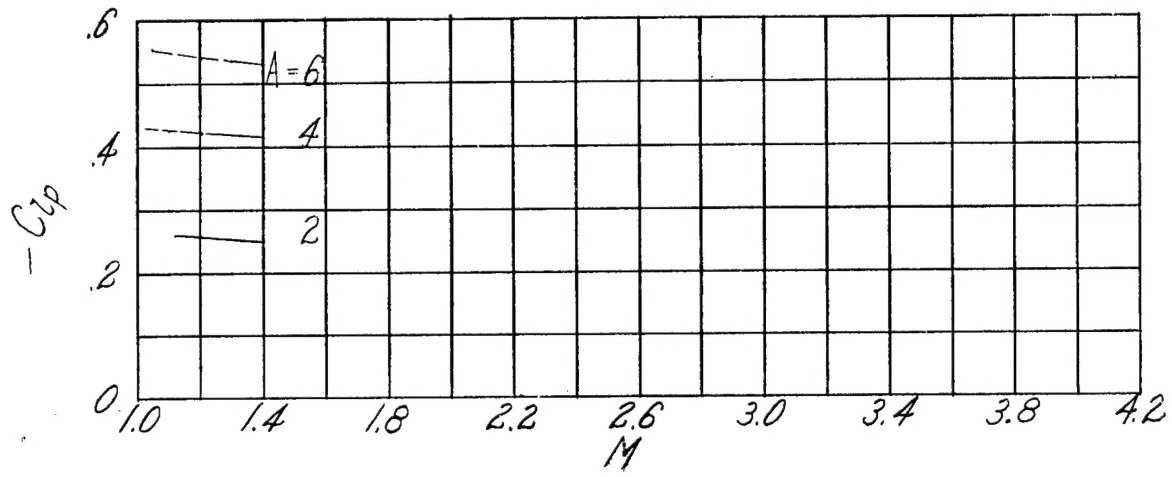

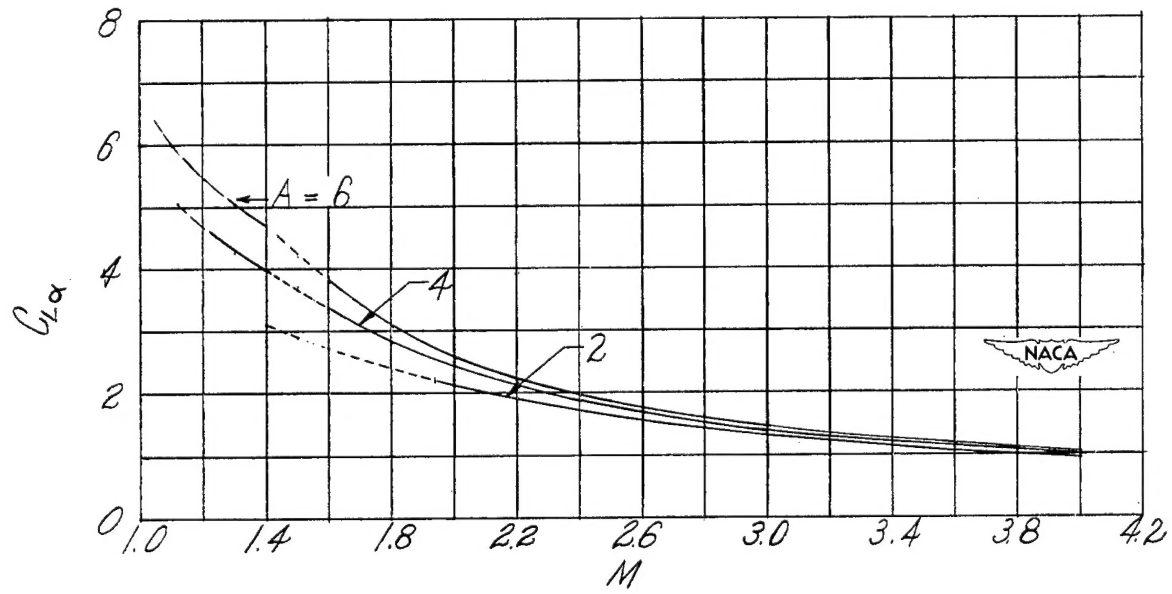

(b) Angle of sweep, 45°.

Figure 16.– Continued.

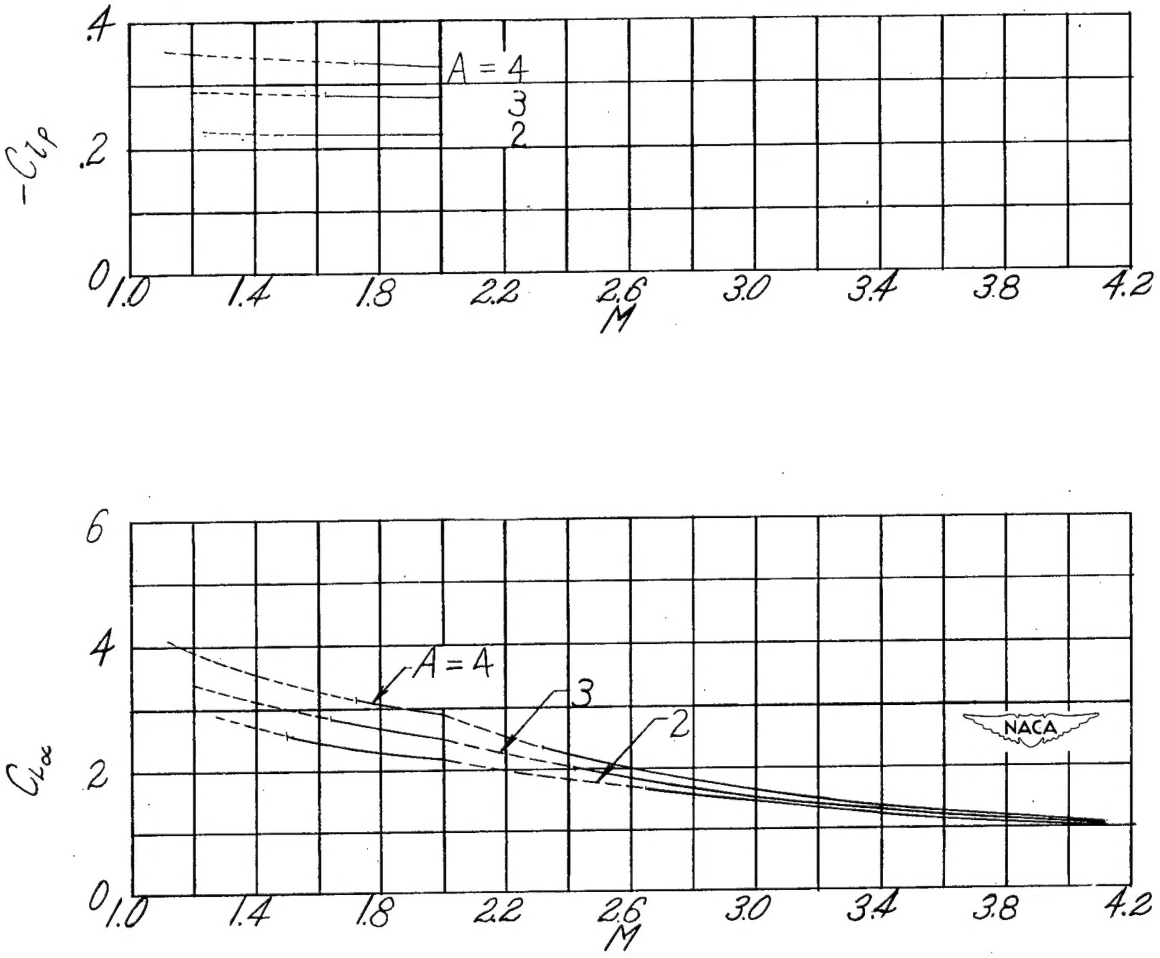

(c) Angle of sweep, 60°.

Figure 16.– Concluded.